The Astronomical Journal, 168:272 (19pp), 2024 December https://doi.org/10.3847/1538-3881/ad8345

BSN: The First Photometric Study of 10 Contact Binary Systems from the Northern and Southern Hemispheres

Atila Poro[1], Kai Li[2], Raul Michel[3], Angel Castro[3], Eduardo Fernández Lajús[4], Li-Heng Wang[2], Jean-François Coliac[5], Yasemin Aladağ[6], Ailar Alizadehsabegh[7], and Fahri Alicavus[8,9]
[1] Binary Systems of South and North (BSN) Project, Tehran, Iran; atilaporo@bsnp.info
[2] Shandong Key Laboratory of Optical Astronomy and Solar-Terrestrial Environment, School of Space Science and Physics, Institute of Space Sciences, Shandong University, Weihai, Shandong 264209, People's Republic of China
[3] Observatorio Astronómico Nacional, Universidad Nacional Autónoma de México, Apartado Postal 877, Ensenada C.P. 22800, B.C., Mexico
[4] Instituto de Astrofísica de La Plata (CCT La Plata-CONICET-UNLP), La Plata, Argentina
[5] Double Stars Committee, Société Astronomique de France, Paris, France
[6] Space Science and Solar Energy Research and Application Center (UZAYMER), University of Çukurova, 01330, Adana, Türkiye
[7] Department of Photonics, University of Tabriz, Tabriz, Iran
[8] Çanakkale Onsekiz Mart University, Faculty of Arts and Sciences, Department of Physics, 17020, Çanakkale, Türkiye
[9] Çanakkale Onsekiz Mart University, Astrophysics Research Center and Ulupnar Observatory, 17020, Çanakkale, Türkiye
Received 2024 June 25; revised 2024 September 22; accepted 2024 October 1; published 2024 November 18

Abstract

Photometric observations were made with standard filters in four observatories for 10 contact binary systems. We analyzed the orbital period variations of the systems and found that six of them show long-term changes. The increase in the orbital period of the J07, N65, and PU Vir systems is caused by mass transfer, and the reduction in the orbital period of the J05, LO Psc, and N49 systems is caused by the combination of angular momentum loss and mass transfer. The first light-curve analysis was performed with the PHysics Of Eclipsing BinariEs Python code and Markov Chain Monte Carlo. We discussed the accuracy of photometric mass ratio estimates for contact binary systems with total and partial eclipses compared to spectroscopic results. We also compared our mass ratio findings to a recent method that estimates mass ratios from the light curve's third derivative. Then, we also discussed this new mass ratio estimate method for photometric data. The systems' positions were displayed in 18 empirical parameter relationships. According to the light-curve analysis and estimation of absolute parameters, systems BE Mus, J07, J08, N49, and N65 are A subtypes, and the others are W subtypes.

Unified Astronomy Thesaurus concepts: Close binary stars (254); CCD photometry (208); Contact binary stars (297); Fundamental parameters of stars (555); Astronomy data analysis (1858)

Materials only available in the online version of record: data behind figure, figure set, machine-readable table

1. Introduction

W Ursae Majoris (W UMa) eclipsing binary systems are crucial objects for studying the structure and formation of stars, stellar evolution theories, and the physical characteristics of stars (S. Qian 2003; K. Yakut & P. P. Eggleton 2005; L. Li et al. 2007; Z. Eker et al. 2008; P. P. Eggleton 2012; A. Poro et al. 2024b). Many significant issues about contact binaries still exist after decades, including the orbital period cutoff (X.-D. Zhang & S.-B. Qian 2020), the stability of systems with very low mass ratios (P. S. Williams & I. W. Roxburgh 1976; K. Li et al. 2022; S. S. Wadhwa et al. 2024), the accurate determination of mass ratios using photometric light curves (S. Kouzuma 2023), and the empirical relationships between parameters like the orbital period–mass ratio or mass–luminosity (A. Poro et al. 2022b, 2024b), all of which require further investigation.

W UMa–type eclipsing contact binary systems contain two stars sharing a common convective envelope (L. B. Lucy 1968a, 1968b). These stars are around the main sequence, with spectral types of F to K. Contact binary systems show a continuous light variation and a small difference between the depths of the two minima (S. B. Qian et al. 2014). The temperatures of two stars in contact systems are close (G. P. Kuiper 1941), and the higher the fillout factor, the more equilibrium can be expected. According to the O. Latković et al. (2021) study, if both conditions, including a higher orbital period than 0.5 day and an effective temperature of 7000 K, exist, that system will not be classified as a W UMa type. Therefore, it can be found in a simple search that most of the systems studied so far have an effective temperature range of about 3500–7200 K.

Contact binary systems have a short orbital period, mostly around 0.2–0.6 day. Contact binaries have a sharp orbital period cutoff of about 0.22 day (S. M. Rucinski 1992; K. Li et al. 2019, 2020). Also, other systems were discovered with even shorter orbital periods (e.g., D. T. F. Weldrake et al. 2004; A. J. Drake et al. 2014a; L. Jiang et al. 2015). The reasons for the orbital period cutoff are far from clear yet. Despite the theoretical studies, increasing and analyzing the number of contact systems in the orbital period cutoff range is necessary. On the other hand, the accurate determination of the orbital period can have an impact on other statistical and experimental parameter relationships/theories for determining the absolute parameters of stars, such as mass (S. Qian 2003; A. Poro et al. 2022b).

Contact binaries are divided into A and W subtypes (L. Binnendijk 1970). The more massive component is a hotter star in the A subtype, and if the less massive component has a higher effective temperature, it is classified as a W subtype. Specifying the subtype depends on which star we consider primary. However, S. Csizmadia & P. Klagyivik (2004) suggested the B subtype for W UMa contact binaries. B-subtype systems' temperature difference between components is more than 1000 K, and they are also referred to as poor thermal contact binaries (S. M. Rucinski 2000). These categorizations for subtypes are still under discussion, and in some cases, it is challenging to distinguish subtypes.

In this study, 10 contact binary systems from the Southern and Northern Hemispheres were investigated. We used ground-based photometric observations, along with the Transiting Exoplanet Survey Satellite (TESS; G. R. Ricker et al. 2015) data for some systems. The ground-based observations were conducted by four observatories in the Binary Systems of South and North (BSN[10]) project. The selected target systems range in apparent magnitude from 11.57 to 16.13, with a short orbital period of 0.209 to 0.337 day. Light-curve analysis is not performed on these systems in the literature, and it is useful to investigate them. The empirical studies of parameter relationships require a suitable, accurate, and significant number of analyzed contact binary systems (A. Poro et al. 2024b).

The first light-curve analysis and estimating the absolute parameters of the target binary systems have been the main parts of this work. Finally, a discussion and conclusion on the systems are presented.

2. Target Systems

We have analyzed 10 binary stars classified in the All Sky Automated Survey for SuperNovae (ASAS-SN; B. J. Shappee et al. 2014; T. Jayasinghe et al. 2018) and AAVSO Variable Star indeX (VSX) catalogs as contact systems. These targets include BE Mus, CSS J050736.0+214218 (hereinafter J05), CSS J072227.8+443027 (hereinafter J07), CSS J081118.7+320828 (hereinafter J08), LO Psc, NSVS 4908885 (hereinafter N49), NSVS 6527318 (hereinafter N65), OT UMa, PU Vir, and V0801 And. The introductions of the target systems are as follows.

1. *BE Mus*. P. Guthnick & R. Prager (1933) presented an ephemeris for this system for the first time, and they announced the orbital period as 0.3369219 day. Additionally, the P. Guthnick & R. Prager (1933) study reported a maximum apparent magnitude of $V_{\max} = 13.3$ mag for BE Musca. The General Catalogue of Variable Stars (GCVS; O. Y. Malkov et al. 2006) and the Catalogue of Eclipsing Variables (E. A. Avvakumova et al. 2013) classify BE Mus as a Southern Hemisphere contact binary system. Gaia DR3 reported 5961 K for BE Mus's effective temperature.
2. *J05*. This binary system was discovered by the Catalina Surveys Data Release-1 (CSDR1; A. J. Drake et al. 2014b). The CSDR1 and ASAS-SN catalogs reported orbital periods of 0.2339980 and 0.2094278 day, respectively. In addition to the difference in the orbital period in catalogs CSDR1 and ASAS-SN, they reported the mean magnitude in the V filter as $V_{\rm CSDR1} = 14.78(25)$ mag and $V_{\rm ASAS-SN} = 16.03(40)$ mag. Looking at the TESS Input Catalog (TIC) v8.2 ($V_{\rm TESS} = 16.199(355)$ mag), it seems that the results of ASAS-SN are more reliable. Gaia DR3 and TIC presented $T_{\rm GaiaDR3} = 4136$ K and $T_{\rm TIC} = 4001(123)$ K for J05. Therefore, this system can be classified as a low-temperature contact binary star.
3. *J07*. The CSDR1 discovered J07 and reported an orbital period of 0.226522 day. J07 was included in the Asteroid Terrestrial-impact Last Alert System (ATLAS) REFCAT2 catalog (J. L. Tonry et al. 2018), and its apparent magnitudes were given in the g, r, i, z, J, H, and K bands. The Zwicky Transient Facility (ZTF; E. C. Bellm et al. 2019; F. J. Masci et al. 2019) catalog also classifies J07 as a contact binary system (X. Chen et al. 2020). The effective temperature of J07 is reported by the Gaia DR3 as 4678 K.
4. *J08*. This system was discovered by the CSDR1, and an orbital period of 0.246884 day was determined. Catalogs ATLAS, ZTF, and ASAS-SN have reported J08 as a contact binary system. J08 was included in a sample of 9380 contact binaries using the Catalina Real-Time Transient Survey Variables Sources Catalogue (F. M. Marsh et al. 2017). According to F. M. Marsh et al. (2017), the system's effective temperature is 4667 K, while Gaia DR3 and TIC reported 4904 K and 4504(107), respectively.
5. *LO Psc*. This binary system was discovered by the ROTSE-I telescope and included in a catalog of 1022 bright contact binary stars presented in the S. J. Gettel et al. (2006) study. The study by D. I. Hoffman et al. (2009) classified LO Pisces as a contact binary system. D. Terrell et al. (2012) reported a BVR_cI_c survey of 606 W UMa binary stars and presented $B-V$, $V-R_c$, R_c-I_c, and $V-I_c$. They determined $V_{\max}$ as 10.94 mag and an orbital period of 0.3455752 day. TIC has presented a temperature of 5554 K for LO Psc; however, Gaia DR3 has not specified any value.
6. *N49*. CSDR1 was discovered in this system. N49 is classified as a contact binary in the ASAS-SN, VSX, ZTF, and ATLAS catalogs. The VSX database reported $V_{\max} = 13.45$ mag for this system. The ZTF variables catalog presented a time of minimum and an orbital period of 0.2441638 day for N49. The temperatures of the N49 binary system have been presented to be 4395 K in the Gaia DR3 and 4386(129) K in the TIC.
7. *N65*. The N65 binary system was identified in the Northern Sky Variability Survey as a W UMa type with an orbital period of 0.26417 day (D. I. Hoffman et al. 2009). For this system, the VSX database presented $V_{\max} = 13.24$ mag. N65 is also classified as a contact binary system in the ZTF, ASAS-SN, and ATLAS catalogs. Gaia DR3 and TIC reported the effective temperature of the system as 5243 K and 5439(186) K, respectively.
8. *OT UMa*. An ephemeris was provided by the Peremennye Zvezdy Prilozhenie database (A. V. Khruslov 2007). GCVS and VSX reported the same $V_{\max} = 12.22$ mag for OT Ursa Major. The ASAS-SN, VSX, GCVS, WISE, and ZTF catalogs have classified OT UMa as a contact binary system. The ZTF variables catalog presented a time of minimum and an orbital period of 0.3160738 day for this target. The reported Gaia DR3 effective temperature for OT UMa is 5769 K, and this parameter's value is 5643 (142) K from the TIC.

[10] https://bsnp.info/

Table 1
Specifications of the Target Systems

System	2MASS	R.A. (J2000)	Decl.(J2000)	d (pc)	V_{max}
BE Mus	012210592−6630324	185.274399	−66.509041	502.43(3.45)	13.56(17)
J05	05073605+2142186	76.900318	21.705154	308.42(3.16)	16.13(21)
J07	07222780+4430280	110.615799	44.507746	673.62(11.44)	15.12(11)
J08	08111879+3208279	122.828232	32.141005	373.27(37.40)	14.40(15)
LO Psc	00532822+2536229	13.367713	25.606332	255.64(1.46)	11.57(9)
N49	10202456+4306412	155.102411	43.111422	287.70(1.59)	13.99(10)
N65	02265165+2935160	36.715283	29.587658	412.36(4.17)	13.53(9)
OT UMa	08192313+6612364	124.846027	66.209919	359.89(1.62)	12.49(8)
PU Vir	012394855−0226216	189.952494	−2.439391	204.09(0.99)	12.37(13)
V0801 And	02000913+4302429	30.037984	43.045356	234.71(1.10)	12.33(11)

Note. Coordinates and distances come from the Gaia DR3.

Table 2
Specifications of the Ground-based Observations

System	Observation(s) Date	Filter	Exposure Time(s)	Binning	Observatory
BE Mus	2024 Mar 10	BVR_cI_c	B(60), V(20), R_c(20), I_c(15)	5 × 5	CASLEO
J05	2023 Dec 7	BVR_cI_c	B(20), V(10), R_c(7), I_c(7)	2 × 2	SPM
J07	2024 Jan 27	BVR_cI_c	B(60), V(30), R_c(10), I_c(10)	2 × 2	SPM
J08	2024 Jan 30	BVR_cI_c	B(60), V(30), R_c(10), I_c(10)	2 × 2	SPM
LO Psc	2023 Oct 13, 2023 Oct 23	VR_c	V(180), R_c(120)	2 × 2	UZAYMER
N49	2024 Jan 26	BVR_cI_c	B(60), V(30), R_c(10), I_c(10)	2 × 2	SPM
N65	2023 Nov 22	VR_cI_c	V(120), R_c(60), I_c(30)	2 × 2	SPM
OT UMa	2023 Feb 10, 2023 Jan 26	VI_c	V(30), I_c(30)	4 × 4	OABAC
PU Vir	2024 Mar 8	BVR_cI_c	B(30), V(10), R_c(8), I_c(8)	5 × 5	CASLEO
V0801 And	2023 Nov 15, 2023 Nov 17	BVR_c	B(60), V(60), R_c(60)	4 × 4	OABAC

9. *PU Vir*. This target was found by L. Bernasconi to be a variable (C. Rinner et al. 2003). The C. Rinner et al. (2003) study presented the first ephemeris with an orbital period of 0.2562555(14) day, and they recognized PU Virgo as a contact system. Additionally, the GCVS, ASAS-SN, and VSX databases classified PU Vir as a contact binary star. The ASAS variable stars in the Southern Hemisphere (ASAS3) catalog reported $V_{max} = 12.10$ mag. An effective temperature of 4967 K by Gaia DR3 and 5107(108) K by TIC are reported for this system.
10. *V0801 And*. The TAROT robotic observatory in France discovered V0801 And with an orbital period of 0.266628 day (Y. Damerdji et al. 2007). V0801 Andromeda was classified as a contact binary system by the ASAS-SN, VSX, ATLAS, and GCVS catalogs. The GCVS catalog reported $V_{max} = 11.95$ mag for this system. Gaia DR3 and TIC presented an effective temperature of 4890 K and 5009(193) K for this system, respectively.

3. Observation and Data Reduction

Photometric observations and data reductions were made with different standard filters for 10 target systems in four observatories in the Northern and Southern Hemispheres. These observations were carried out on 13 nights during the years 2023 and 2024 (Table 2).

We considered the air mass with a formula from the W. A. Hiltner (1962) study and a Python code based on the Astropy package (Astropy Collaboration et al. 2013, 2018, 2022) for all of the ground-based observations. Additionally, air-mass correction was applied to the observational data, and the flux was normalized using the AstroImageJ (AIJ) software (K. A. Collins et al. 2017).

Table 1 contains the coordinates and distance from Gaia DR3 (Gaia Collaboration et al. 2023) and the V_{max} determined from our observations. The observational information for each of the systems is presented in Table 2. Table 3 lists the comparisons and checks stars and their coordinates from Gaia DR3.

3.1. Complejo Astronomico El Leoncito Observatory

The observations of BE Mus and PU Vir were made using the 2.15 m Jorge Sahade telescope at the Complejo Astronomico El Leoncito (CASLEO) Observatory, Argentina (69°18′ W, 31°48′ S, 2552 m above sea level). A CCD Versarray 2048B, Roper Scientific, Princeton Instruments, and standard BVR_cI_c filters were employed. Also, a scale of $0\farcs15$ pixel^{-1} and binning of 5 × 5 were used for observations.

The APPHOT photometry package of IRAF[11] was used for CCD reduction and aperture photometry (D. Tody 1986). These processes were conducted using bias and flat-field images.

3.2. San Pedro Martir Observatory

The five binary systems J05, J07, J08, N49, and N65 were observed at the San Pedro Martir (SPM) Observatory in Mexico. This observatory is located at longitude 115°27′49″ W, latitude 31°02′39″ N and an altitude of 2830 m above sea level. The following equipment was utilized for the observations: a 0.84 m Ritchey–Chrétien telescope ($f/15$), a Mexman filter

[11] http://iraf.noao.edui

Table 3
List of Comparison and Check Stars in the Observations

System	Star Type	Star Name	R.A. (J2000)	Decl. (J2000)
BE Mus	Comparison	2MASS J12211813−6631487	185.325515	−66.530221
BE Mus	Check	2MASS J12210234−6628597	185.259632	−66.483271
J05	Comparison	2MASS J05071636+2142372	76.818244	21.710333
J05	Check	2MASS J05073432+2142251	76.893094	21.707007
J07	Comparison	2MASS J07221823+4428562	110.575967	44.482269
J07	Check	2MASS J07221944+4430316	110.581053	44.508790
J08	Comparison	2MASS J08112004+3211048	122.833391	32.184544
J08	Check	2MASS J08110665+3211533	122.777705	32.198174
LO Psc	Comparison	TYC 1742-1501-1	13.436793	25.710722
LO Psc	Comparison	TYC 1742-1865-1	13.284319	25.555827
LO Psc	Check	TYC 1742-1793-1	13.491318	25.595772
N49	Comparison	2MASS J10200956+4306382	155.039629	43.110361
N49	Check	2MASS J10200956+4306382	155.074415	43.143527
N65	Comparison	2MASS J02270218+2933004	36.759139	29.550072
N65	Check	2MASS J02270206+2935412	36.758645	29.594799
OT UMa	Comparison	Gaia DR3 1093610793684777472	124.785057	66.362352
OT UMa	Check	Gaia DR3 1093555680664518656	124.844945	66.150794
PU Vir	Comparison	2MASS J12395360−0226443	189.973376	−2.445676
PU Vir	Comparison	SDSS J123954.17−022503.7	189.975830	−2.417822
PU Vir	Check	TYC 4948-1040-1	189.982445	−2.373548
V0801 And	Comparison	Gaia DR3 346511368669282048	30.023625	43.049184
V0801 And	Check	Gaia DR3 346524391010108544	29.920890	43.150740

Note. Coordinates come from the Gaia DR3.

wheel, a Spectral Instruments CCD detector (e2v CCD42-40 chip with $13.5 \times 13.5\,\mu 2$ pixels, gain of $1.39e-$ ADU^{-1}, and readout noise of $3.54e-$), and BVR_cI_c standard filters.

All the images were processed using IRAF[12] routines (D. Tody 1986). Images were bias subtracted, flat-field corrected, and aligned before the instrumental magnitudes were computed with the standard aperture photometry method using an aperture of 1.5 times the average FWHM of each object's images.

3.3. UZAYMER Observatory

The observations of LO Psc were carried out by a 0.5 m Ritchey–Chrétien RC 500/4000 Pro RC SGA OTA ($f/8$) telescope at the UZAYMER Observatory, Çukurova University, Adana, Türkiye (longitude 35°21'19" N, latitude 37° 03'35" E, and altitude of 130 m). We used a Finger Proline Instruments PL16803 type CCD with 4096×4096 pixels and a $9\,\mu$m pixel size. The CCD temperature average during observations was −30°C. Observations were conducted using standard filters V and R_c.

The standard process was employed for performing basic data reduction using bias, dark, and flat fields on the raw CCD images. We aligned, reduced, and plotted raw images with AIJ software (K. A. Collins et al. 2017).

3.4. Observatoire Astronomique des Binaires André Coliac Observatory

The OT UMa and V0801 And binary systems were observed at the Observatoire Astronomique des Binaires André Coliac (OABAC) observatory in Marseille, France (longitude 05° 27'56" E, latitude 43°18'54" N). We used a Newton 200 mm ($f/4$) telescope with a field corrector in the observation process.

An ASI ZWO 183MM Pro with standard VI_c filters for OT UMa and an ASI ZWO 533MM Pro CCD with standard BVR_c filters were applied for V0801 And. The average CCD temperature for both systems' observations was 0°C.

We employed FotoDif[13] and Siril[14] software for the standard data reduction process, using dark, bias, and flat fields on the images.

3.5. TESS Observations

NASA launched TESS in 2018 with the goal of discovering exoplanets (G. R. Ricker et al. 2010; K. G. Stassun et al. 2018). Four wide-field cameras on this space telescope allow it to observe different parts of the sky. TESS observes a designated region of the sky during each sector for 27.4 day. We used time-series available TESS data for the BE Mus, J08, LO Psc, N49, N65, OT UMa, and V0801 And binary systems. "TESS: T" is used as a passband in these systems' light-curve analysis process, covering a broadband wavelength range of 600–1000 nm (G. R. Ricker et al. 2015). Table 4 lists the TESS sectors used in this study.

TESS data are available at the Mikulski Archive for Space Telescopes (MAST).[15] TESS-style curves were extracted from MAST using the LightKurve[16] code. The data were detrended using the TESS Science Processing Operations Center pipeline (J. M. Jenkins et al. 2016).

[12] IRAF is distributed by the National Optical Astronomy Observatories, operated by the Association of Universities for Research in Astronomy, Inc., under a cooperative agreement with the National Science Foundation.

[13] http://www.astrosurf.com/orodeno/fotodif/

[14] https://siril.org/

[15] https://mast.stsci.edu/portal/Mashup/Clients/Mast/Portal.htmL

[16] https://lightkurve.github.io/lightkurve/

Table 4
TESS Data Specifications Used in This Study

System	TIC	TESS Sector	Exposure Time (s)	Obs. Year
BE Mus	448018469	11, 37, 38, 64, 65	1800, 600, 600, 200, 200	2019, 2021, 2023
J08	165834549	20, 44, 45, 46, 47	1800, 600, 600, 600, 600	2019, 2020, 2021, 2022
LO Psc	13935976	17, 57	1800, 200	2019, 2022
N49	150229405	21, 48	1800, 600	2020, 2022
N65	21182129	18, 58	1800, 200	2019, 2022, 2023
OT UMa	99680466	20, 47, 60	1800, 600, 200	2020, 2022, 2023
V0801 And	291955609	18, 58	1800, 200	2019, 2022

4. Orbital Period Variations

We tried to collect as many times of minima as possible from photometric surveys, the ASAS-SN, ZTF, TESS, and Wide Angle Search for Planets (SuperWASP; O. W. Butters et al. 2010), to assist in analyzing the orbital period variations of these 10 targets. In addition, we also collected data from AAVSO and the $O-C$ gateway.[17] For TESS 2 minute cadence data, SuperWASP, and AAVSO continuous observation data, we can directly calculate their eclipse timings. However, for the TESS 10 and 30 minute cadence data, ZTF, and ASAS-SN dispersed data, we used the period shift method suggested by K. Li et al. (2020) to obtain their eclipse timings. The K. K. Kwee & H. van Woerden (1956) method was applied to calculate the times of eclipse. Since both the Barycentric Julian Date in Barycentric Dynamical Time ($\mathrm{BJD_{TDB}}$) and the Heliocentric Julian Date (HJD) are present in the data, we first used an online tool[18] to convert them all to $\mathrm{BJD_{TDB}}$. The extracted times of minima are listed in Table 5. Then, we calculated the $O-C$ values using the linear ephemeris (Equation (1)),

$$\mathrm{BJD_{TDB}} = \mathrm{BJD_{TDB0}} + P \times E. \tag{1}$$

$\mathrm{BJD_{TDB}}$ is the observational times of eclipse, $\mathrm{BJD_{TDB0}}$ is the initial primary eclipsing time, and P is the orbital period. Figure 1 displays the $O-C$ diagrams. It is apparent from this figure that six stars show parabolic variations, whereas four systems have linear variations. Equation (2) was used to fit the $O-C$ diagrams,

$$O - C = \Delta T_0 + \Delta P_0 \times E + \frac{\beta}{2}E^2. \tag{2}$$

The fitted parameters are shown in Table 6. We found that three stars show a long-term increase in their orbital periods, while three stars show a long-term decrease in their orbital periods. Based on the fitted parameters (Table 6), the new ephemerides were obtained and listed in Table 7.

The long-term increase in the orbital period is usually caused by mass transfer from the less massive component to the more massive component, while the continuous orbital period decrease generally results from mass transfer from the more massive component to the less massive one or from angular momentum loss (AML) or their combination. Using the following equation from the K. K. Kwee (1958) study,

$$\frac{\dot{P}}{P} = -3\dot{M}\left(\frac{1}{M_1} - \frac{1}{M_2}\right). \tag{3}$$

We calculated the mass transfer rate for the target systems as shown in Table 6. For J05, LO Psc, and N49, their orbital periods are continuously decreasing, and the more massive component is losing mass. We use the equation $\tau_{\mathrm{th}} = \frac{GM_m^2}{R_m L_m}$ to calculate the thermal timescale for them, and $\tau_{\mathrm{th}} = 2.02 \times 10^8$ yr for J05, $\tau_{\mathrm{th}} = 4.00 \times 10^7$ yr for LO Psc, and $\tau_{\mathrm{th}} = 1.22 \times 10^8$ yr for N49 are obtained. The thermal mass transfer rate (J. W. Lee et al. 2004; X.-Y. Liu et al. 2023) was calculated to be $M_m/\tau_{\mathrm{th}} = 3.75 \times 10^{-9}\ M_\odot\,\mathrm{yr}^{-1}$ for J05, $M_m/\tau_{\mathrm{th}} = 2.80 \times 10^{-8}\ M_\odot\,\mathrm{yr}^{-1}$ for LO Psc, and $M_m/\tau_{\mathrm{th}} = 5.57 \times 10^{-9}\ M_\odot\,\mathrm{yr}^{-1}$ for N49 (M_m means the mass of the more massive component). These three values differ significantly from those calculated in Table 6, implying that the mass transfer does not occur via the thermal timescale. Then, we calculated the orbital period decrease rate caused by AML using the following equation that the E. F. Guinan & D. H. Bradstreet (1988) study provided,

$$\frac{\dot{P}}{P} \approx -1.1 \times 10^{-8} q^{-1}(1+q)^2(M_p + M_s)^{-5/3}k^2 \times (M_p R_p^4 + M_s R_s^4)P^{-7/3}, \tag{4}$$

where P is the orbital period, q is the mass ratio, M_p is the primary mass, M_s is the secondary mass, R_p is the primary radius, R_s is the secondary radius, and k is the dimensionless gyration radius ($k_{1,2}^2 = 0.06$ was used following L. Li & F. Zhang 2006). Then, $dp/dt = -1.53 \times 10^{-8}$ days yr^{-1} for J05, $dp/dt = -5.26 \times 10^{-8}$ days yr^{-1} for LO Psc, and $dp/dt = -1.74 \times 10^{-8}$ days yr^{-1} for N49 were obtained, and the values differ significantly from the actual orbital period change rate. Therefore, AML alone cannot explain the orbital period decrease. The combination of AML and mass transfer should be the reason.

It should be noted that the absolute parameters, such as the mass and radius of the stars used in this section's calculations, were followed by the estimations presented in Section 6 of this study.

5. Light-curve Solutions

We prepared the ground-based and TESS data for the light-curve analysis process. For this purpose, we used the most recent TESS sector if each system's data were available. Light-curve analyses of the target binary systems were carried out using the PHysics Of Eclipsing BinariEs (PHOEBE) Python code version 2.4.9 and the Markov Chain Monte Carlo

[17] http://var2.astro.cz/ocgate/
[18] https://astroutils.astronomy.osu.edu/time/hjd2bjd.html

Table 5
The Times of Minima Extracted from Our Observations and Space-based Data and Collected from the Literature

System	Min. (BJD_{TDB})	Epoch	$O - C$	Source	System	Min. (BJD_{TDB})	Epoch	$O - C$	Source
BE Mus	2457849.9743(9)	−7508	−0.0229	ASAS-SN	N49	2457375.0222(7)	−12126.5	0.0087	ASAS-SN
	2457850.1414(8)	−7507.5	−0.0243	ASAS-SN		2457375.1419(14)	−12126	0.0063	ASAS-SN
	2458600.1502(6)	−5281.5	−0.0161	TESS		2458873.5838(1)	−5989	0.0125	TESS
	2458600.3179(7)	−5281	−0.0169	TESS		2458873.7052(1)	−5988.5	0.0118	TESS
	2460059.0606(4)	−951.5	−0.0018	TESS		2458880.0534(1)	−5962.5	0.0118	TESS
	2460059.2255(3)	−951	−0.0054	TESS		2458880.1761(1)	−5962	0.0124	TESS
	2460379.6489(4)	0	0	This study		2458888.1109(1)	−5929.5	0.0118	TESS
	2460379.8189(2)	0.5	0.0015	This study		2458888.2339(1)	−5929	0.0127	TESS
						2458894.5822(1)	−5903	0.0128	TESS
J05	2457724.2720(18)	−12230.5	0.0005	ASAS-SN		2458894.7032(1)	−5902.5	0.0117	TESS
	2458635.1780(5)	−7881	0.0003	ZTF		2459615.0992(1)	−2952	0.0012	TESS
	2458635.2839(5)	−7880.5	0.0015	ZTF		2459615.2280(1)	−2951.5	0.0080	TESS
	2459187.1261(7)	−5245.5	0.0014	ZTF		2459619.1346(1)	−2935.5	0.0079	TESS
	2459187.2315(8)	−5245	0.0021	ZTF		2459619.2504(1)	−2935	0.0017	TESS
	2460285.6782(3)	0	0	This study		2459630.1221(1)	−2890.5	0.0081	TESS
	2460285.7825(3)	0.5	−0.0004	This study		2459630.2372(1)	−2890	0.0011	TESS
	2460285.8870(4)	1	−0.0006	This study		2459634.1439(1)	−2874	0.0012	TESS
	2460285.9924(3)	1.5	0.0001	This study		2459634.2727(1)	−2873.5	0.0079	TESS
						2460335.8707(3)	0	0	This study
J07	2457031.4468(8)	−14591.5	−0.0162	ASAS-SN		2460335.9982(4)	0.5	0.0054	This study
	2457031.5618(12)	−14591	−0.0145	ASAS-SN					
	2458010.4749(19)	−10269.5	−0.0192	ASAS-SN	N65	2453205.6882(6)	−26744	−0.0358	SuperWASP
	2458010.5912(27)	−10269	−0.0162	ASAS-SN		2454076.4146(10)	−23448	−0.0302	SuperWASP
	2458625.1538(3)	−7556	−0.0096	ZTF		2460270.8202(2)	0	0	This study
	2458625.2668(3)	−7555.5	−0.0099	ZTF		2460270.9522(2)	0.5	−0.0001	This study
	2459625.1435(4)	−3141.5	−0.0044	ZTF					
	2459625.2570(5)	−3141	−0.0042	ZTF	OT UMa	2456729.3520(10)	−10257.5	−0.0558	$O - C$ gateway
	2460336.7690(3)	0	0	This study		2456729.3523(10)	−10257.5	−0.0555	$O - C$ gateway
	2460336.8830(3)	0.5	0.0007	This study		2456729.3527(10)	−10257.5	−0.0551	$O - C$ gateway
						2456729.5096(3)	−10257	−0.0562	$O - C$ gateway
J08	2454084.6242(15)	−25336.5	−0.0182	SuperWASP		2459944.6033(1)	−85	0.0041	TESS
	2457200.0496(8)	−12717.5	−0.0081	ASAS-SN		2459944.7619(1)	−84.5	0.0046	TESS
	2457200.1716(10)	−12717	−0.0095	ASAS-SN		2459971.4650(5)	0	0	This study
	2458050.0665(8)	−9274.5	−0.0090	ASAS-SN		2459986.3209(8)	47	0.0008	This study
	2458050.1889(8)	−9274	−0.0101	ASAS-SN					
	2459528.5308(1)	−3286	−0.0030	TESS	PU Vir	2452407.5148(50)	−31102.5	−0.0621	$O - C$ gateway
	2459528.6550(2)	−3285.5	−0.0022	TESS		2457174.9210(16)	−12498.5	−0.0332	ASAS-SN
	2460339.7910(4)	0	0	This study		2457175.0401(10)	−12498	−0.0423	ASAS-SN
	2460339.9140(3)	0.5	−0.0004	This study		2458050.0376(21)	−9083.5	−0.0292	ASAS-SN
						2458050.1582(11)	−9083	−0.0367	ASAS-SN
LO Psc	2453202.6855(4)	−20339.5	0.0070	SuperWASP		2459125.4284(18)	−4887	−0.0145	ZTF
	2453206.6597(4)	−20328	0.0072	SuperWASP		2459715.7250(10)	−2583.5	−0.0026	$O - C$ gateway
	2453216.6801(8)	−20299	0.0061	SuperWASP		2460377.7636(2)	0	0	This study
	2453219.6169(3)	−20290.5	0.0056	SuperWASP		2460377.8957(2)	0.5	0.0040	This study
	2459857.6135(2)	−1081.5	0.0058	TESS					
	2459857.7864(2)	−1081	0.0058	TESS	V0801 And	2454397.4671(10)	−22001.5	−0.0197	SuperWASP
	2460231.3385(6)	0	0	This study		2454397.6016(10)	−22001	−0.0185	SuperWASP
	2460231.5121(7)	0.5	0.0008	This study		2460264.2968(5)	0	0	This study
	2460241.3594(5)	29	−0.0006	This study		2460264.4317(4)	0.5	0.0015	This study
	2460241.5319(4)	29.5	−0.0008	This study		2460266.2979(5)	7.5	0.0011	This study

Note.
(This table is available in its entirety in machine-readable form in the online article.)

(MCMC) approach (A. Prša et al. 2016; K. E. Conroy et al. 2020). According to the classification of the target systems in the catalogs, we used contact mode for light-curve analysis, considering that contact binary systems are indicated by the short orbital period and shape of light curves. We also calculated each system's phase shift relative to the reference ephemeris, which includes the referent times of minimum (t_0) obtained from our observations in this study and the orbital period from the catalogs (Table 7). As listed in Table 8, the phase shifts are small, and the primary and secondary minima can be distinguished.

It was assumed that $g_1 = g_2 = 0.32$ (L. B. Lucy 1967) and $A_1 = A_2 = 0.5$ (S. M. Ruciński 1969) were the gravity-darkening coefficients and the bolometric albedo, respectively. The stellar atmosphere was modeled using the F. Castelli & R. L. Kurucz (2004) method, and the limb-darkening coefficients were employed as free parameters in PHOEBE.

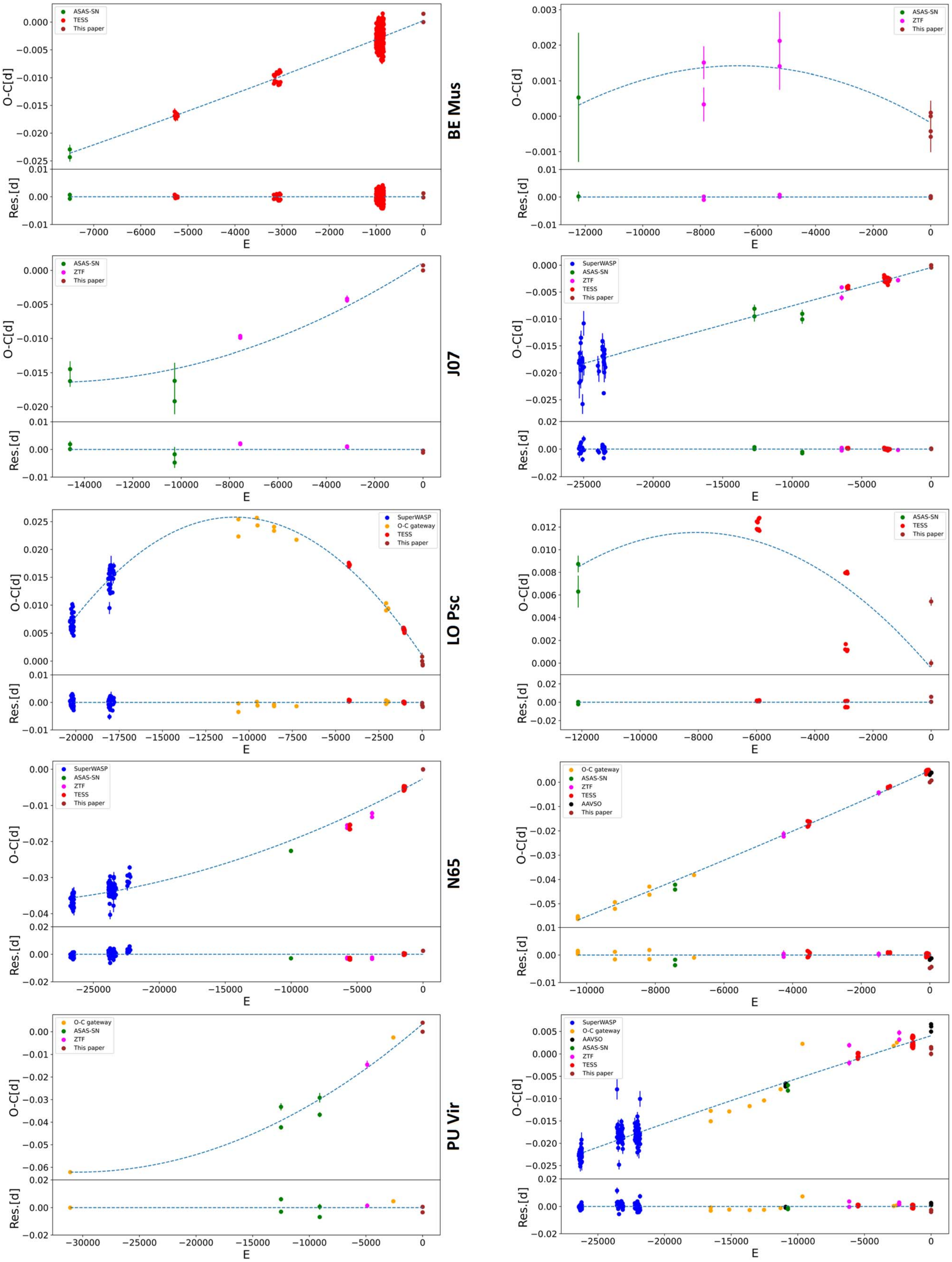

Figure 1. The $O - C$ diagrams of the target binary systems.

Table 6
The $O - C$ Fitting Coefficients and Mass Transfer Rate

System	ΔT_0 ($\times 10^{-4}$ days)	Error	ΔP_0 ($\times 10^{-7}$ days)	Error	β ($\times 10^{-7}$ days yr^{-1})	Error	dM_1/dt ($\times 10^{-7} M_\odot$ yr^{-1})	Error
BE Mus	1.05	2.83	0.32	1.88	0	0	0	0
J05	−1.86	5.85	−4.81	2.75	−1.25	0.88	−3.29	2.30
J07	11.61	31.47	7.36	10.30	2.37	2.20	49.89	46.34
J08	−4.41	6.63	7.12	0.42	0	0	0	0
LO Psc	9.98	2.26	−45.87	1.28	−4.48	0.13	3.05	0.10
N49	−4.35	39.30	−29.69	14.21	−5.51	3.25	342.91	201.89
N65	25.65	3.38	19.91	1.50	0.78	0.16	−0.51	0.10
OT UMa	46.86	1.59	60.42	0.58	0	0	0	0
PU Vir	34.43	56.79	43.03	10.37	2.01	0.92	−31.12	14.23
V0801 And	41.67	2.52	9.97	0.17	0	0	0	0

Table 7
Reference and New Ephemeris of the Systems

System	Reference Ephemeris		New Ephemeris	
	t_0/Source	Period/Source	Corrected t_0	New Period
BE Mus	2460379.6489(4)	0.3369275/ASAS-SN	2460379.64903(28)	0.33692753(19)
J05	2460285.6782(3)	0.2094278/ASAS-SN	2460285.67799(59)	0.20942732(28)
J07	2460336.7690(3)	0.2265227/ASAS-SN	2460336.77016(315)	0.22652344(103)
J08	2460339.7910(4)	0.2468829/ASAS-SN	2460339.79056(66)	0.24688361(4)
LO Psc	2460231.3385(6)	0.345567/VSX	2460231.33947(23)	0.34556241(13)
N49	2460335.8707(3)	0.2441642/ASAS-SN	2460335.87024(393)	0.24416123(142)
N65	2460270.8202(2)	0.264175/ASAS-SN	2460270.82276(34)	0.26417699(15)
OT UMa	2459971.4650(5)	0.316067/VSX	2459971.46966(16)	0.31607304(6)
PU Vir	2460377.7636(2)	0.2562555/ASAS-SN	2460377.76703(568)	0.25625980(104)
V0801 And	2460264.2968(5)	0.266655/VSX	2460264.30100(25)	0.26665600(2)

Note. The referent times of minimum (t_0) were obtained from our observations in this study.

Table 8
Light-curve Solutions of the Target Binary Systems

Parameter	BE Mus	J05	J07	J08	LO Psc	N49	N65	OT UMa	PU Vir	V0801 And
T_1 (K)	$5939^{+(11)}_{-(9)}$	$4139^{+(11)}_{-(11)}$	$4702^{+(6)}_{-(7)}$	$4862^{+(7)}_{-(6)}$	$5368^{+(8)}_{-(8)}$	$4177^{+(8)}_{-(11)}$	$5195^{+(7)}_{-(9)}$	$5906^{+(6)}_{-(7)}$	$5125^{+(11)}_{-(12)}$	$4514^{+(7)}_{-(7)}$
T_2 (K)	$5916^{+(10)}_{-(12)}$	$4162^{+(11)}_{-(9)}$	$4572^{+(6)}_{-(5)}$	$4989^{+(7)}_{-(7)}$	$5140^{+(10)}_{-(8)}$	$4432^{+(7)}_{-(7)}$	$5259^{+(7)}_{-(7)}$	$5454^{+(11)}_{-(8)}$	$4809^{+(10)}_{-(13)}$	$4726^{+(6)}_{-(7)}$
$q = M_2/M_1$	$0.976^{+(13)}_{-(9)}$	$0.693^{+(17)}_{-(14)}$	$0.959^{+(17)}_{-(13)}$	$1.364^{+(16)}_{-(11)}$	$2.394^{+(13)}_{-(10)}$	$1.009^{+(12)}_{-(15)}$	$3.019^{+(23)}_{-(27)}$	$1.600^{+(12)}_{-(15)}$	$1.057^{+(25)}_{-(24)}$	$0.628^{+(6)}_{-(5)}$
i (deg)	$61.40^{+(4)}_{-(4)}$	$59.24^{+(4)}_{-(6)}$	$68.73^{+(5)}_{-(4)}$	$64.56^{+(4)}_{-(4)}$	$89.80^{+(7)}_{-(7)}$	$52.53^{+(25)}_{-(4)}$	$76.50^{+(4)}_{-(4)}$	$62.16^{+(4)}_{-(3)}$	$41.64^{+(8)}_{-(6)}$	$74.52^{+(3)}_{-(5)}$
f	$0.100^{+(5)}_{-(3)}$	$0.191^{+(3)}_{-(5)}$	$0.120^{+(3)}_{-(2)}$	$0.034^{+(4)}_{-(3)}$	$0.357^{+(4)}_{-(3)}$	$0.047^{+(3)}_{-(3)}$	$0.125^{+(4)}_{-(4)}$	$0.061^{+(3)}_{-(3)}$	$0.119^{+(4)}_{-(4)}$	$0.105^{+(4)}_{-(3)}$
$\Omega_1 = \Omega_2$	3.658(7)	3.155(5)	3.620(4)	4.302(3)	5.583(5)	3.739(6)	6.564(8)	4.639(5)	3.777(6)	3.076(5)
$l_1/l_{\rm tot}$	$0.509^{+(1)}_{-(1)}$	$0.573^{+(1)}_{-(1)}$	$0.557^{+(1)}_{-(1)}$	$0.391^{+(1)}_{-(1)}$	$0.356^{+(1)}_{-(1)}$	$0.436^{+(1)}_{-(1)}$	$0.257^{+(1)}_{-(1)}$	$0.463^{+(1)}_{-(1)}$	$0.584^{+(1)}_{-(1)}$	$0.553^{+(1)}_{-(1)}$
$l_2/l_{\rm tot}$	0.491(1)	0.427(1)	0.443(1)	0.609(1)	0.644(1)	0.564(1)	0.743(1)	0.537(1)	0.416(1)	0.447(1)
$r_{\rm (mean)1}$	0.391(3)	0.428(4)	0.395(3)	0.356(3)	0.332(3)	0.384(4)	0.296(2)	0.344(3)	0.386(4)	0.430(4)
$r_{\rm (mean)2}$	0.387(3)	0.364(3)	0.388(3)	0.410(4)	0.482(5)	0.385(3)	0.486(5)	0.427(4)	0.396(4)	0.348(3)
Phase shift	0.005(1)	0.000(1)	−0.004(1)	0.000(1)	0.017(1)	0.051(1)	−0.019(1)	0.013(1)	0.000(1)	0.013(1)
Starspot										
Col. (deg)	$112.7^{+(1.1)}_{-(1.3)}$	$123.1^{+(1.6)}_{-(1.8)}$	$107.3^{+(1.1)}_{-(0.9)}$	$106.6^{+(1.5)}_{-(1.1)}$		$121.9^{+(7)}_{-(9)}$	$93.0^{+(1.2)}_{-(1.2)}$		$103.5^{+(1.2)}_{-(1.3)}$	$105.5^{+(1.5)}_{-(8)}$
Long. (deg)	$309.4^{+(1)}_{-(1)}$	$66.5^{+(1.4)}_{-(1.6)}$	$320.5^{+(1.1)}_{-(0.9)}$	$20.5^{+(1.2)}_{-(1.2)}$		$46.3^{+(1.1)}_{-(1.1)}$	$43.6^{+(1.0)}_{-(9)}$		$302.4^{+(2.1)}_{-(2.1)}$	$256.6^{+(7)}_{-(9)}$
Radius (deg)	$17.2^{+(2)}_{-(2)}$	$14.8^{+(3)}_{-(3)}$	$24.1^{+(2)}_{-(2)}$	$13.9^{+(3)}_{-(3)}$		$12.2^{+(2)}_{-(2)}$	$12.1^{+(2)}_{-(2)}$		$18.4^{+(3)}_{-(2)}$	$23.1^{+(1)}_{-(2)}$
$T_{\rm spot}/T_{\rm star}$	$0.923^{+(3)}_{-(4)}$	$0.873^{+(4)}_{-(5)}$	$0.881^{+(3)}_{-(4)}$	$0.950^{+(2)}_{-(2)}$		$0.940^{+(5)}_{-(4)}$	$0.868^{+(4)}_{-(5)}$		$0.880^{+(4)}_{-(5)}$	$0.777^{+(5)}_{-(5)}$
Star	Secondary	Secondary	Secondary	Secondary		Secondary	Secondary		Secondary	Secondary

We obtained the input effective temperature (T) to start the analysis process from the Gaia DR3 database. Gaia DR3 did not present the temperature for the LO Psc system, and the TIC report was used. This temperature was set according to the depth of minima on the hotter star of the system. We estimated the initial effective temperature of the other component by

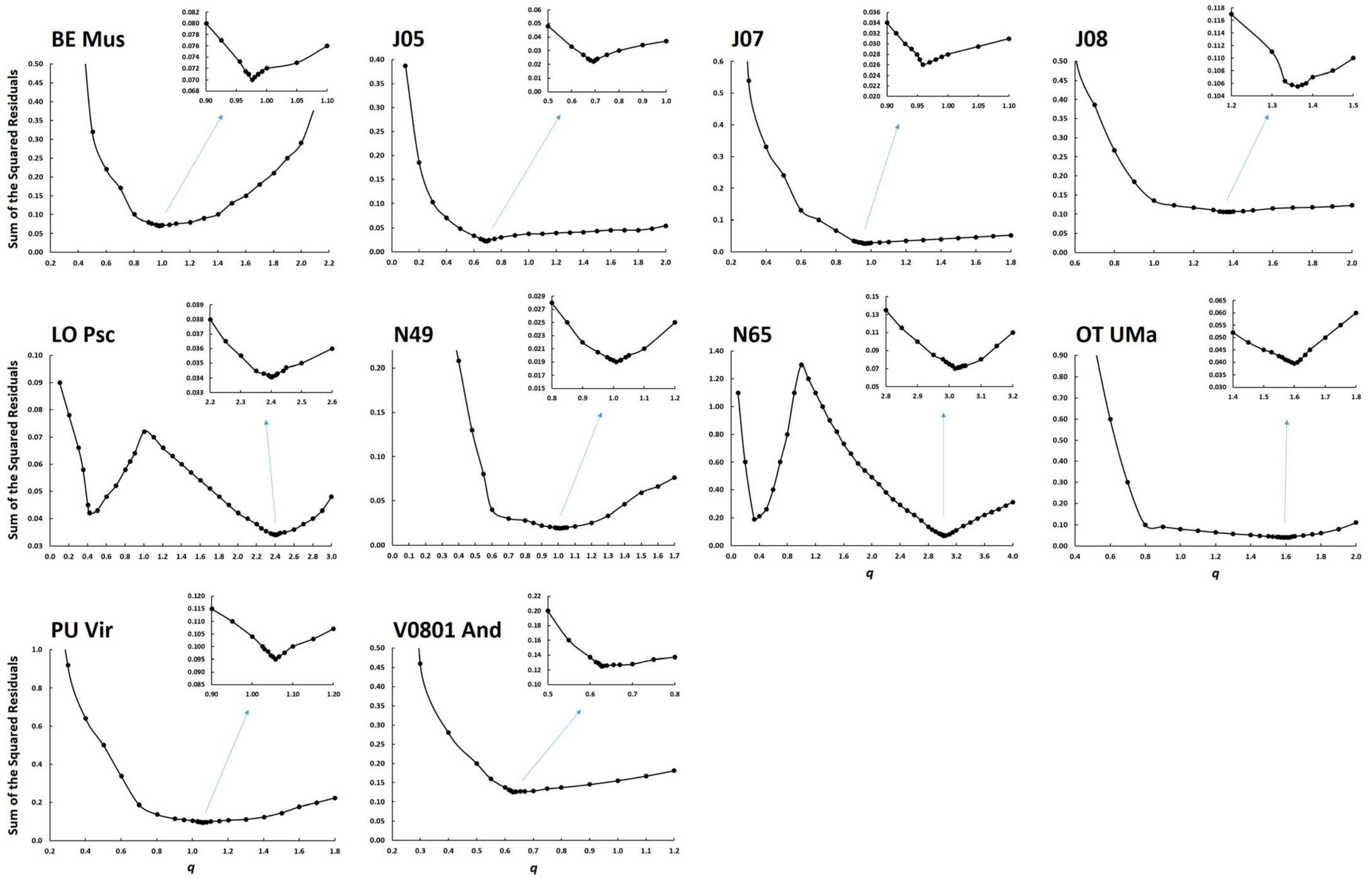

Figure 2. Sum of the squared residuals as a function of the mass ratio. The zoomed part is shown with an arrow.

using the difference in the depth of the primary and secondary minima.

We used the q-search method to estimate the mass ratio of the systems (D. Terrell & R. E. Wilson 2005). We searched a range of mass ratios between 0.1 and 10 for all target systems. Then, we shortened the interval and searched again according to the minimum sum of squared residuals. Figure 2 illustrates that each q-search curve has a clear minimum sum of squared residuals, and we estimated initial values of mass ratios.

The well-known O'Connell effect (D. J. K. O'Connell 1951) is indicated by the asymmetry in the brightness of maxima in the light curve of eclipsing binary stars. The presence of magnetic activity on the star's surface could be a possible explanation for this phenomenon, which causes the existence of a starspot. Due to the apparent magnitude difference in the maxima, eight target systems needed a starspot in the light-curve solutions (Table 8). Colatitude, longitude, angular radius, and the ratio of temperature are the characteristics that are commonly identified for a starspot (Table 8).

Considering that the presence of a starspot on the systems may affect the results of the initial values, we repeated the q-search process to be sure. Then, we tried to determine the acceptable theoretical fit on the observation data by using the initial values obtained for $T_{1,2}$, q, f, and i. Additionally, we employed PHOEBE's optimization tool to improve the output of light-curve solutions and yield the intended results.

The MCMC approach based on the emcee package (D. Foreman-Mackey et al. 2013) was used to obtain the final values of the parameters and their uncertainty. Therefore, six main parameters, i, q, f, $T_{1,2}$, and l_1, along with four starspot parameters, if any, were considered for the MCMC modeling process. We set the appropriate Gaussian distribution to cover the entire observational light curve. We employed 96 walkers and 5000 iterations for 10 binary systems. Through the process of light-curve analysis, l_3 was not detected in the target systems.

Table 8 presents the outcomes of the light-curve solutions, and Figure 3 shows the corner plot of the N65 system as an example that was determined by MCMC modeling. Figure 4 displays the binary systems' observed and final synthetic light curves. The rest of the corner plots of other target systems are available. The 3D representation of the binary systems and the starspots on the stars are displayed in Figure 5.

6. Fundamental Parameters

The accuracy of absolute parameter estimations is significant for investigating the evolution of contact systems and parameter relationships (A. Poro et al. 2024b). So, various methods are used to calculate the absolute parameters of the contact binary systems. The Gaia DR3 parallax is one of the methods used for this estimation when only photometric data are available (K. Li et al. 2021), and it was described in detail by the A. Poro et al. (2024a) study. This method of estimating absolute parameters has two other influential parameters, including the interstellar extinction A_V and $V_{\max}$. The accuracy of $V_{\max}$ is related to the observations' process, and a large value for the A_V parameter makes it hard to expect proper accuracy in estimating absolute parameters using the Gaia DR3 parallax.

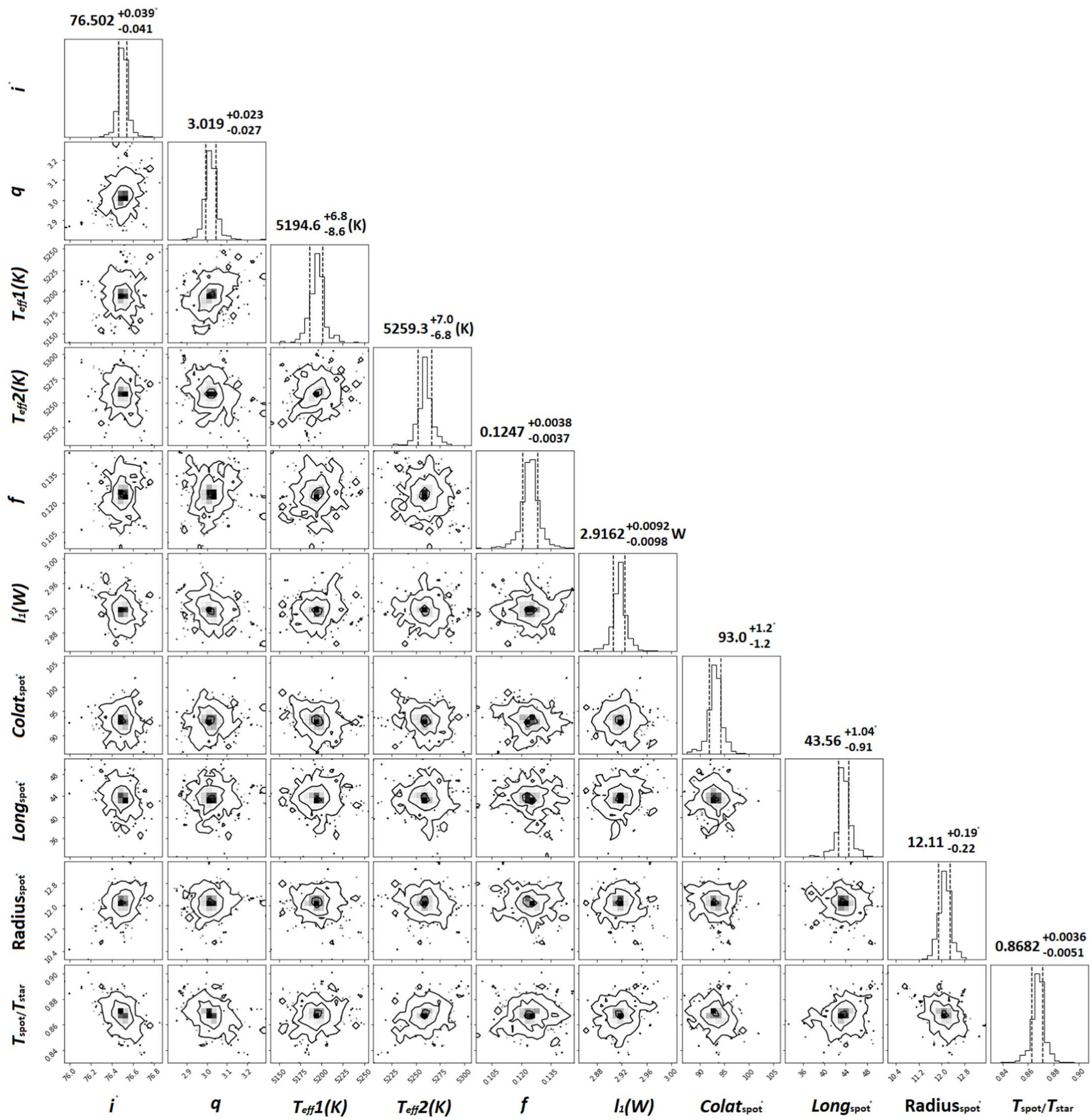

Figure 3. The corner plots of the N65 system were determined by MCMC modeling.
(The complete figure set (10 images) is available in the online article.)

We calculated A_V from the 3D dust map based on the Gaia distance (G. M. Green et al. 2019). Therefore, systems BE Mus, J05, and J07 have inappropriate A_V values (Table 9) to use the Gaia DR3 parallax to this estimation. Therefore, it was inevitable to use another method dependent on the empirical parameter relationship to estimate the absolute parameters of the target systems.

A. Poro et al. (2024c) updated the orbital period and semimajor axis ($P{-}a$) empirical relationship using 414 contact binary systems with orbital periods less than 0.7 day (Equation (5)):

$$a = (0.372^{+0.113}_{-0.114}) + (5.914^{+0.272}_{-0.298}) \times P. \quad (5)$$

The estimation process for the absolute parameters started with Equation (5). Therefore, each target system's orbital period was used to obtain the value of a ($R_\odot$). We used the mass ratio (q) from the light-curve solutions and Kepler's well-known third law equation to estimate the mass and uncertainty

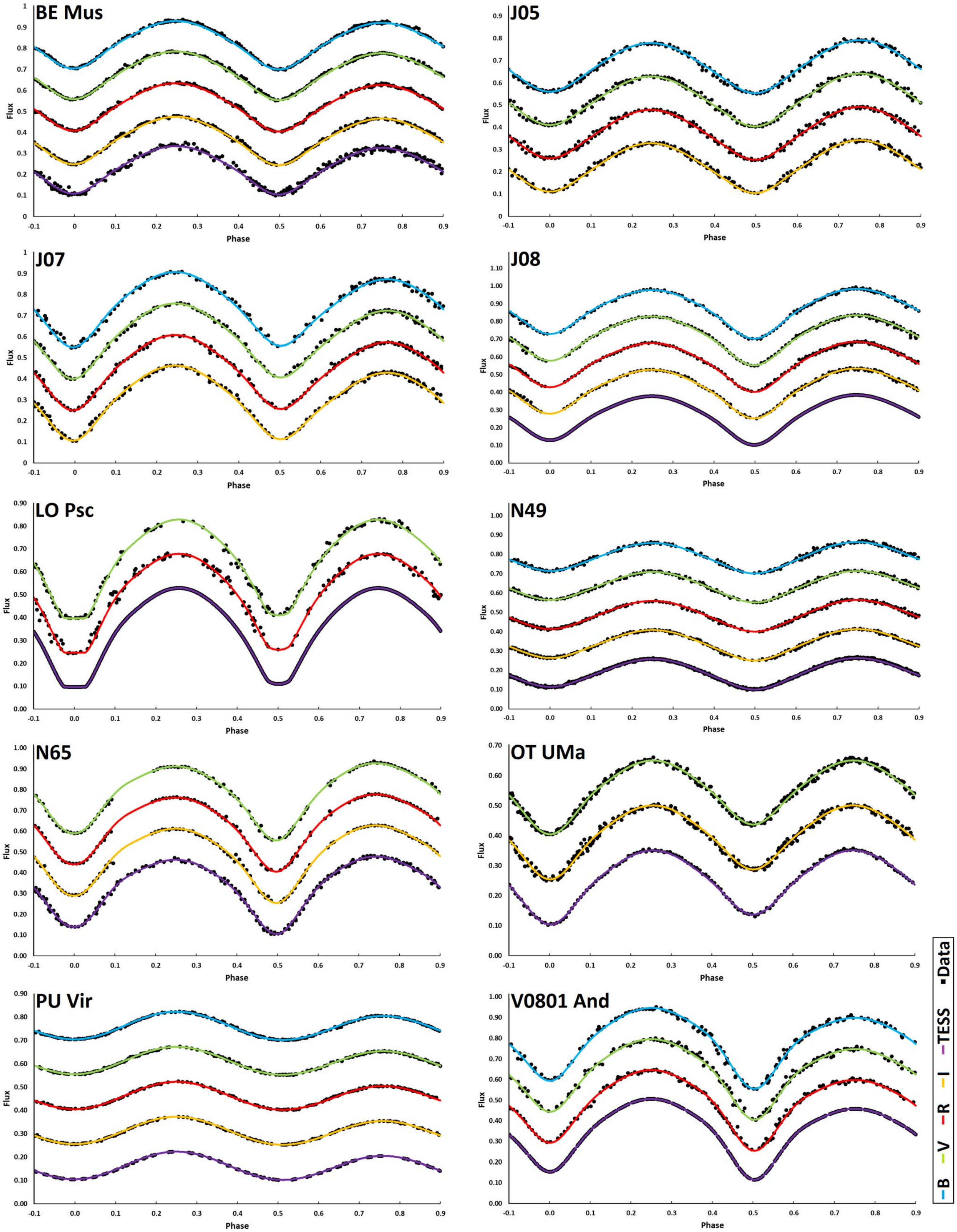

Figure 4. The black dots show the observed light curves of the systems, and the synthetic light curves were generated using the light-curve solutions. From top to bottom, the filters are B, V, R_c, I_c, and TESS, as shown by the colors. The B, V, R_c, and I_c photometry is available as the data behind the figure for all 10 systems. (The data used to create this figure are available in the online article.)

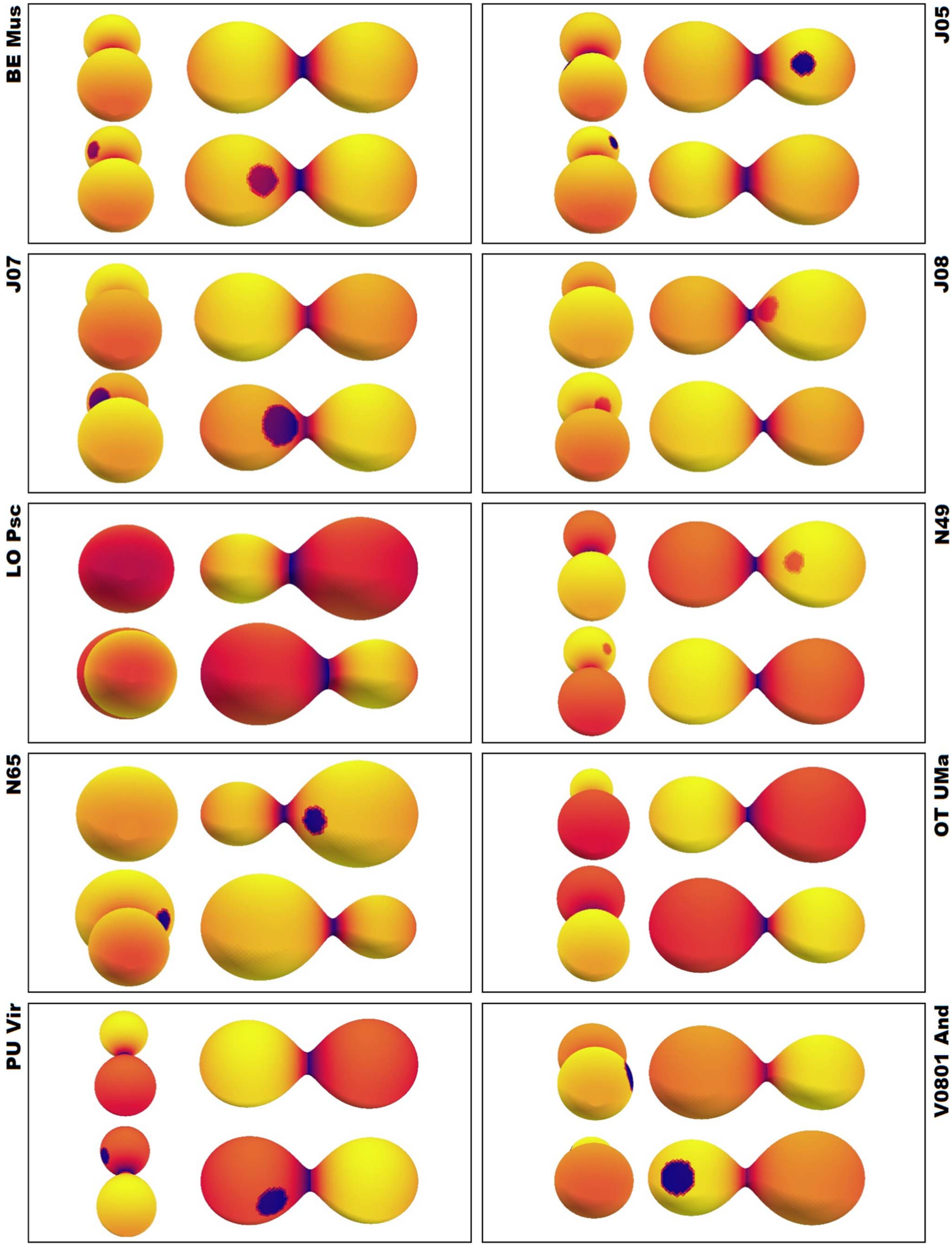

Figure 5. 3D view of stars in the binary systems. The color represents the effective temperature variations on the star's surface.

Table 9
Estimated Absolute Parameters of the Systems

Parameter	BE Mus	J05	J07	J08	LO Psc	N49	N65	OT UMa	PU Vir	V0801 And
M_1 ($M_\odot$)	0.79(23)	0.76(27)	0.67(23)	0.57(19)	0.47(13)	0.67(22)	0.35(11)	0.58(17)	0.67(22)	0.86(28)
M_2 ($M_\odot$)	0.77(24)	0.52(20)	0.64(24)	0.78(27)	1.12(33)	0.68(24)	1.05(35)	0.93(29)	0.71(25)	0.54(18)
R_1 ($R_\odot$)	0.92(9)	0.69(8)	0.68(8)	0.65(7)	0.80(8)	0.70(8)	0.57(6)	0.77(8)	0.73(8)	0.84(9)
R_2 ($R_\odot$)	0.92(9)	0.59(7)	0.66(7)	0.75(8)	1.16(12)	0.70(8)	0.94(10)	0.96(10)	0.75(8)	0.68(7)
L_1 ($L_\odot$)	0.96(20)	0.13(3)	0.20(5)	0.21(5)	0.48(10)	0.13(3)	0.22(5)	0.65(14)	0.33(8)	0.26(6)
L_2 ($L_\odot$)	0.92(20)	0.09(2)	0.17(4)	0.32(8)	0.85(18)	0.17(4)	0.61(14)	0.73(16)	0.27(7)	0.21(5)
M_{bol1} (mag)	4.78(21)	6.98(25)	6.47(24)	6.40(23)	5.52(21)	6.92(24)	6.40(22)	5.19(21)	5.93(24)	6.18(23)
M_{bol2} (mag)	4.82(21)	7.31(25)	6.63(24)	5.98(23)	4.90(21)	6.65(23)	5.27(23)	5.07(22)	6.15(24)	6.44(23)
M_{V1} (mag)	4.83(21)	7.92(24)	6.93(23)	6.78(23)	5.70(21)	7.81(23)	6.63(22)	5.25(21)	6.19(23)	6.77(22)
M_{V2} (mag)	4.87(21)	8.22(24)	7.18(23)	6.30(23)	5.15(21)	7.31(23)	5.47(23)	5.22(21)	6.56(23)	6.89(22)
$\log(g)_1$(cgs)	4.40(3)	4.64(4)	4.60(4)	4.57(3)	4.30(3)	4.58(3)	4.46(3)	4.43(3)	4.54(3)	4.53(3)
$\log(g)_2$(cgs)	4.40(4)	4.62(5)	4.60(4)	4.58(4)	4.35(3)	4.58(4)	4.51(4)	4.44(3)	4.54(4)	4.51(4)
a ($R_\odot$)	2.36(21)	1.61(17)	1.71(18)	1.83(18)	2.42(21)	1.82(18)	1.93(19)	2.24(20)	1.89(19)	1.95(19)
BC_1	−0.054(2)	−0.938(13)	−0.464(4)	−0.374(3)	−0.173(2)	−0.894(11)	−0.229(3)	−0.059(1)	−0.255(5)	−0.589(5)
BC_2	−0.057(1)	−0.911(12)	−0.548(4)	−0.313(3)	−0.250(4)	−0.652(6)	−0.207(2)	−0.149(3)	−0.402(6)	−0.449(4)
A_V	0.405(2)	0.731(2)	0.248(1)	0.085(4)	0.078(1)	0.037(1)	0.209(1)	0.073(1)	0.067(1)	0.118(1)

of each star (Equations (6) and (7)):

$$M_1 = \frac{4\pi^2 a^3}{GP^2(1+q)}, \tag{6}$$

$$M_2 = q \times M_1. \tag{7}$$

The radius (R) of each companion was calculated using $r_{\mathrm{mean}1,2}$ from the light-curve solutions and the equation $R = a \times r$. The effective temperature and radius of each star make it possible to calculate the luminosity of the components.

The luminosity was employed to determine the absolute bolometric magnitude (M_{bol}) by utilizing the relationship between the stellar parameters (Equation (8)):

$$M_{\mathrm{bol}1,)} = M_{\mathrm{bol}\odot} - 2.5 \times \log\left(\frac{L_{1,2}}{L_\odot}\right). \tag{8}$$

The Sun's absolute bolometric magnitude is considered to be 4.73 mag based on the G. Torres (2010) study. The absolute magnitude (M_V) value of the stars in the target systems was also calculated using the bolometric correction (BC) from the P. J. Flower (1996) study and the equation $M_V = M_{\mathrm{bol}} - \mathrm{BC}$. Then, we estimated the surface gravity (g) of the stars on a logarithmic scale using the M and R parameters. The results of estimating 10 binary systems' absolute parameters are presented in Table 9.

7. Discussion and Conclusion

We presented the first light-curve analysis, orbital period variations, and absolute parameter estimations of 10 contact binary systems. These binary systems were observed at four observatories in the Northern and Southern Hemispheres with multiband standard filters. Based on the analysis and results, the following are presented as discussions and conclusions.

(A) The stars in the target systems have a temperature range of 4100–5900 K. The minimum and maximum temperature difference between the two companion stars (ΔT) was found in the BE Mus and J05 systems (23 K) and OT UMa (452 K), respectively (Table 11). Based on the A. N. Cox (2000) and Z. Eker et al. (2018) studies, the effective temperature of the stars indicates that they are in the G and K spectral categories (Table 11).

(B) This study has found that system LO Psc is a total eclipse, while other target systems are partial eclipse binary systems. When a total eclipse occurs in a contact binary system, the parameters of each star can be measured more precisely, so a reliable mass ratio is obtained (J. Kallrath et al. 2009; M. Pešta & O. Pejcha 2023). Therefore, it can be expected that the photometric mass ratio estimation of total eclipse contact binary systems will be acceptable. Can such accuracy be obtained with partial eclipse systems? Some studies statistically compared the mass ratio derived from spectroscopic data (q_{sp}) with photometry data (q_{ph}) and found that the total eclipse systems' trend was closer to the q_{sp} results than partial eclipses (e.g., Ľ Hambálek 2013; K. Li et al. 2021; S. Kouzuma 2023). So, there is a general view that photometric mass ratios cannot be accurately determined for systems that have partial eclipses; this view can be critically examined.

We produced a comparison plot of q_{sp} and q_{ph} by employing 100 contact binary systems from a sample used in the K. Li et al. (2021) study and adding 13 additional systems from the literature (Table 10). In Figure 6, the systems with blue (total eclipse) and green (partial eclipse) colors represent the system used by K. Li et al. (2021), and the systems with red colors are the systems added in this study. We used the $i > \arccos|(r_1 - r_2)/a|$ relationship to determine each system type, and all 13 were partial eclipses (W. Sun et al. 2020). We plotted a linear fit on total eclipsed systems with an uncertainty that was very close to a one-to-one linear fit (Figure 6). As is clear in Figure 6, the systems with a partial eclipse that we added show a behavior similar to the total eclipse systems. Currently, the number of systems that have both q_{sp} and q_{ph} is very limited. Therefore, statistical inferences about the accuracy of the mass ratio of systems with partial eclipses will be improved after having a larger sample with appropriate precision. It is also challenging to select spectroscopic and photometric studies for the sample; ideally, in a study including spectroscopy, both q_{sp} and q_{ph} should be determined.

The study of K. Li et al. (2021) utilized a sample of 101 contact systems; however, we omitted the LS Del study and employed 100 of them. The studies selected for LS Del by the K. Li et al. (2021) sample had mass ratios of $q_{sp} = 0.375$ and $q_{ph} = 0.562$, which have a significant difference from each other to use in Figure 6. So, we selected two other studies

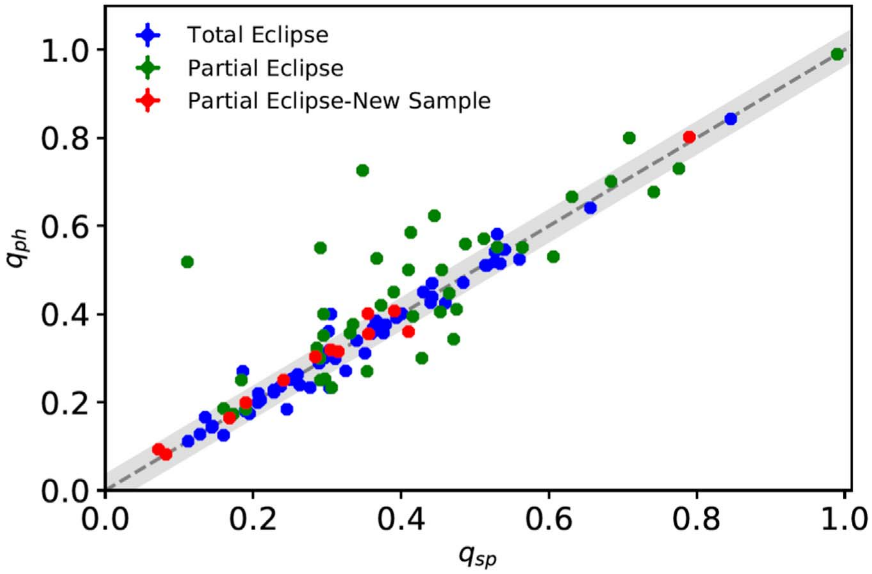

Figure 6. Comparing mass ratio results utilizing spectroscopic (q_{sp}) and photometric (q_{ph}) data for available samples.

Table 10
Contact Binary Systems with Spectroscopic and Photometric Observations

System	P (days)	q_{sp}	q_{ph}	i (deg)	References
YY Crb	0.376565	0.241	0.25	81.5	A. Essam et al. (2010), S. Soomandar & A. Poro (2024)
V870 Ara	0.399773	0.082	0.082	73.6	T. Szalai et al. (2007), A. Poro et al. (2021)
DY Cet	0.440790	0.356	0.355	85.6	T. Pribulla et al. (2009), M. F. Yıldırım (2022)
LO And	0.3804418885	0.305	0.319	80.1	R. H. Nelson & R. M. Robb (2015), H.-P. Huang et al. (2021)
KR Com	0.40797003	0.072	0.093	52.1	T. Mitnyan et al. (2020), K. Gazeas et al. (2021)
V1073 Cyg	0.785850	0.284	0.303	68.4	X.-M. Tian et al. (2018), T. Mitnyan et al. (2020)
V2150 Cyg	0.5918609	0.79	0.802	43.4	J. M. Kreiner et al. (2003), T. Mitnyan et al. (2020)
LS Del	0.363842	0.391	0.407	47.8	T. Mitnyan et al. (2020), A. Poro et al. (2024d),
V972 Her	0.443094	0.168	0.164	40.1	S. O. Selam et al. (2018), T. Mitnyan et al. (2020)
EX Leo	0.4086041	0.19	0.199	60.8	S. Zola et al. (2010), T. Mitnyan et al. (2020)
V351 Peg	0.593297	0.41	0.36	63.0	B. Albayrak et al. (2005), T. Mitnyan et al. (2020)
V357 Peg	0.5784511	0.355	0.401	73.2	S. Deb & H. P. Singh (2011), T. Mitnyan et al. (2020)
EE Cet	0.379925	0.315	0.315	78.5	G. Djurašević et al. (2006), K. Gazeas et al. (2021)

Note. Orbital periods are from the VSX database.

(Table 10) for this partial eclipsing binary system ($i \approx 48°$) that have a closer q_{sp} and q_{ph} to each other. The case of LS Del highlights the challenge of selecting appropriate studies for the samples used in mass ratio (q_{sp}−q_{ph}) comparisons. Most of the selected systems in Table 10 have been chosen from studies whose light-curve analysis has been done in some way using the MCMC method or MC simulation, and they showed good compatibility with the linear fit in Figure 6.

The accuracy of spectroscopic data for mass ratio estimation depends on some factors. Having spectroscopic data is not always meant to estimate the mass ratio with high precision. For example, the spectroscopic results may not be accurate enough when the system's mass ratio is extremely low (K. Sriram et al. 2016). So, the spectroscopic observations need a good resolution of the spectroscopic instrument, telescope aperture, and observation periods for the target binary systems.

(C) S. Kouzuma (2023) suggested a new method to estimate the photometric mass ratio of overcontact binaries using the light curve's derivatives. This method is different from other common iterative methods, such as q-search and MCMC for mass ratio estimation. S. Kouzuma (2023) examined the efficacy of the new method on a sample of systems with spectroscopic mass ratios. S. Kouzuma (2023) found that around 67% of the results by the new method agreed with the spectroscopic mass ratios within the estimated uncertainties and that the errors for 95% of the compared systems were within ±0.1.

The discussed method is based on derivatives at different orders of the photometric light curve. The S. Kouzuma (2023) study used 117,600 synthetic light curves as a sample to discover the use of light-curve derivatives in mass ratio estimation. There are three conditions[19] for using this method, the most important of which is the existence of maxima and minima in the second- and third-order derivatives. After the derivative of the third order is calculated and considering the minimum and maximum times around the eclipse time and the

[19] Due to the details of these conditions to use the method, we request that the reference study be read (S. Kouzuma 2023).

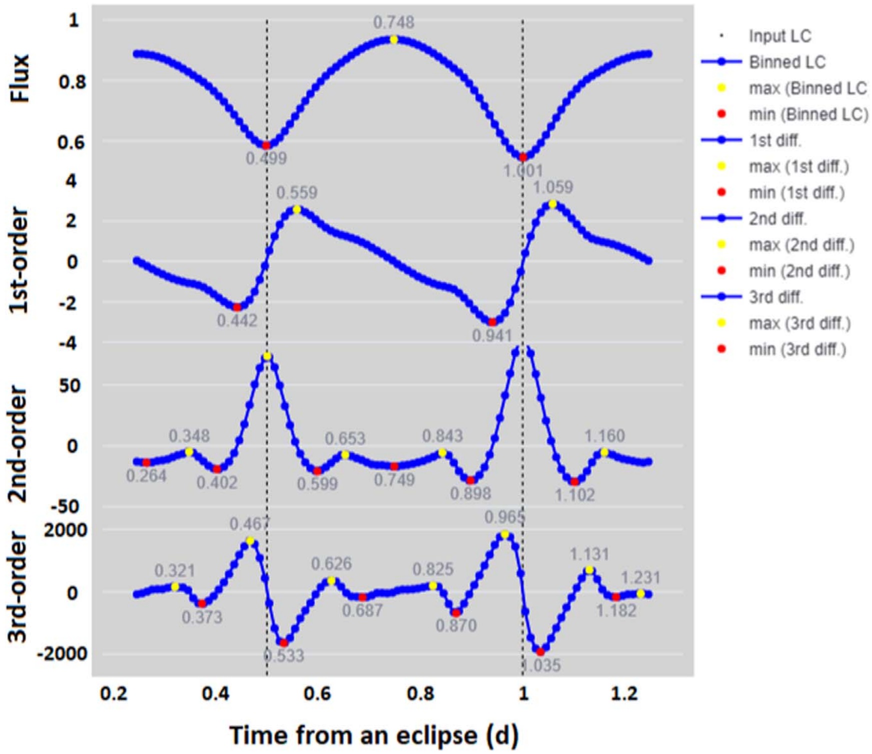

Figure 7. A photometric light curve of V0801 And and first to third derivatives (top to bottom panels, respectively) as an example1 of a process for systems. The units of the panels on the vertical axis from top to bottom are W m^{-2}, 10 W m^{-2} day^{-1}, 10^2 W m^{-2} day^{-2}, and 10^4 W m^{-2} day^{-3}, respectively.

Table 11
Some Specifications and Calculations Regarding Target Systems

Parameter	BE Mus	J05	J07	J08	LO Psc	N49	N65	OT UMa	PU Vir	V0801 And
ΔT (K)	23	23	130	127	228	255	64	452	316	212
Sp. category	G1/G1	K5/K5	K3/K4	K2/K1	K0/K1	K5/K5	K0/K0	G1/G8	K1/K2	K4/K5
$1/q^{*}$[a]	0.976	0.693	0.959	0.733	0.418	0.991	0.331	0.625	0.946	0.628
$1/q^{**}$[b]	…	…	…	0.650	0.384	…	0.422	0.547	…	0.568
$\Delta 1/q$[c]	…	…	…	0.083	0.034	…	0.091	0.078	…	0.060
$M_{\rm tot}$ ($M_\odot$)	1.56(46)	1.28(47)	1.31(47)	1.35(46)	1.58(46)	1.35(46)	1.39(46)	1.51(46)	1.37(47)	1.40(45)
log(J_0)	51.66(19)	51.43(23)	51.47(22)	51.50(21)	51.59(18)	51.50(21)	51.41(20)	51.60(19)	51.52(21)	51.52(20)
M_V (mag)	4.65(15)	7.95(19)	5.73(7)	6.45(6)	4.45(8)	6.66(9)	5.24(7)	4.64(7)	5.75(12)	5.36(8)
System subtype	A	W	A	A	W	A	A	W	W	W

[a] This study.
[b] The obtained values for mass ratio based on the S. Kouzuma (2023) study method.
[c] The difference in mass ratio obtained by the S. Kouzuma (2023) method and this study's results ($1/q$).

system's orbital period, a parameter named W is measured. The S. Kouzuma (2023) investigation revealed a strong relationship between W and q.

We attempted to use the S. Kouzuma (2023) method to estimate the mass ratio for our systems and compared the results with the findings from MCMC and light-curve analysis. We thank Shinjirou Kouzuma, who gave us the ability to use the code for this method. Therefore, it was possible to use this method for these five systems: J08, LO Psc, N65, OT UMa, and V0801 And. The method is not applicable to the other five systems since there was no appearance of a double peak in the second derivative of the light curve. Considering that the mass ratio estimated by the S. Kouzuma (2023) method is present in $1/q$ form, the results are shown in Table 11 for five target systems. Figure 7 also shows the estimation process for the V0801 And system. The difference between the mass ratio obtained in this study and with the S. Kouzuma (2023) method is also shown in Table 11, which shows that all of them are within the uncertainty range of ± 0.1.

Using light-curve derivatives to estimate the photometric mass ratio is a different method and can be effective. We have conducted a review of this new method based on the published study (S. Kouzuma 2023). (1) In the study of the method, there is no mention of the effect of the starspot in the process of estimating the mass ratio. Therefore, we estimated the mass ratio of the five systems in this study with and without a starspot on the light curves. We repeated the same experiment with 21 other contact systems from the accessible data of the J. Rahimi et al. (2021), A. Poro et al. (2022a, 2024c), and E. Paki & A. Poro (2024) studies. The outcomes revealed a change of less than 2% in each instance. Therefore, it can be concluded that the presence of a starspot in the light curve does not interfere with estimating the mass ratio by this method. (2) We used TESS data and ground-based data with different filters for another examination. It was found that the method cannot estimate the mass ratio in cases where the number of data points is small. Also, in most cases, for light curves with the phase horizontal axis, even with a small amount of data scattering, the method cannot estimate the mass ratio for ground-based or TESS data. It is recommended that a part of the TESS data (about 3 or 4 times the orbital period) be used to reduce scattering and obtain more appropriate results, as it is probable that not all 27.4 days of observations in a sector are suitable for use. Therefore, this method is highly sensitive to data dispersion. We suggest that to estimate the mass ratio with this method, it is better to find the best fit with modeling software and use it for the input data. (3) Apart from the three conditions mentioned in the study, this method has limitations that make it unsuitable for some contact systems. It seems that this method is more suitable for total or close-to-total eclipse systems. According to the comparison of the method with the mass ratio from spectroscopic results in the S. Kouzuma (2023) study, it is a suitable and acceptable method for the initial estimation of the mass ratio. However, it is necessary to use methods such as MCMC to improve the mass ratio's accuracy along with other parameters.

(D) Statistical studies have been carried out regarding the mass ratio distribution in the $1/q$ scale of contact binary stars. Except for the cutoff mass ratio region, there is the dispersion of mass ratio in all other parts. This statistical distribution has been done for other parameters, such as the orbital period of contact systems that have a peak in about 0.35 day (X.-Z. Li et al. 2024). According to the analysis of O. Latković et al. (2021), there are two peaks in the mass ratio distribution: one at $q = 0.34$ and the other at $q = 0.83$. Also, X.-Z. Li et al. (2024) concluded that half of the systems have mass ratios between 0.25 and 0.55, with the median at 0.39. On the other hand, X.-Z. Li et al. (2024) reported one peak in $q = 0.25$. We have listed the mass ratios of the studied systems in Table 11 with a scale of $1/q$. The LO Psc and N65 systems are in the range of the first peak, and the rest are in the range or near the second peak of the O. Latković et al. (2021) study.

(E) Figure 8 displays the positions of the 10 studied systems on the 18 parameter relationship diagrams. Based on the light-curve analysis and the estimation of absolute parameters, we presented the evolution state of the 10 systems on the Hertzsprung–Russell, mass–luminosity ($M-L$), and mass–radius ($M-R$) diagrams (Figures 8(a), (b), (d), (e), (g), and (h)). The positions of the stars were displayed in each of these diagrams relative to the zero-age main sequence (ZAMS) and terminal-age main sequence (TAMS) lines. The ZAMS and TAMS lines are from the L. Girardi et al. (2000) study.

The A. Poro et al. (2024d) study used 428 contact binary systems to present the $T_h–M_m$ theoretical fit. The hotter component was identified as T_h and the more massive star as M_m. Based on the star's mass determined by estimating the absolute parameters and the effective temperature obtained from the light-curve analysis, we placed the star's position on the $T_h–M_m$ diagram (Figure 8(c)). There is good agreement between the position of the primary star and this theoretical fit and uncertainty. The gray points in Figure 8(c) are the samples used in the A. Poro et al. (2024d) study, which were compared with the studied systems.

Furthermore, we displayed the star positions on the $\log(g)_1 - \log T_1$ diagram (Figure 8(f)), which was derived from the M. Yıldız (2015) study. In the diagram, the stars are positioned between ZAMS and TAMS, with only LO Psc close to and above the TAMS line.

The orbital angular momentum of each system was estimated using the Z. Eker et al. (2006) study (Equation (9)),

$$J_0 = \frac{q}{(1+q)^2}\sqrt[3]{\frac{G^2}{2\pi}M^5P}, \qquad (9)$$

where q is the mass ratio, M is the total mass of the system, P is the orbital period, and G is the gravitational constant. Table 11 contains a list of the systems' $\log(J_0)$ computation results. According to the values of $M_{\rm tot}$ and $\log(J_0)$ and the theoretical fit of Z. Eker et al. (2006), our systems are in the region of contact binary systems (Figure 8(i)).

The stars' positions in the empirical relationships from the A. Poro et al. (2024b) study were also examined. The positions of the stars are in good agreement with the $P–L_{1,2}$ relationships, as Figures 8(j) and (k) illustrate. Also in these diagrams, we displayed a sample of 118 contact binary systems from the A. Poro et al. (2024b) study that had an orbital period shorter than 0.6 day, and the absolute parameters were estimated based on the Gaia DR3 parallax.

The relationship between the orbital period and mass ($P–M$) of the stars in contact systems has been the subject of numerous statistical investigations (S. Qian 2003; S. Kouzuma 2018; O. Latković et al. 2021; A. Poro et al. 2022b). According to the available samples, there is no strong relationship between these two parameters, but there seems to be a definite trend. So we showed the placement of the 10 target systems on a $P–M$ relationship diagram presented by the A. Poro et al. (2022b) study. Figures 8(m), (n), and (q) show relationships with more massive stars (M_m), less massive stars (M_l), and a total mass of stars ($M_{\rm tot}$). The P and $\log(g)_1$ parameter relationship fit from the A. Poro et al. (2022b) study and our stars' positions on the diagram were also shown in Figure 8(r). The positions of the stars of the target systems are well positioned compared to the theoretical fits.

Additionally, we examined our results on the relationships of the radius ratio and luminosity ratio of the stars with the mass ratio of the systems ($M_2/M_1–R_2/R_1$ and $M_2/M_1–L_2/L_1$). These relationships have come from the A. Poro et al. (2022a, 2024b) studies, respectively. The positions of the stars in the diagrams are in good agreement with the theoretical fits. The gray points in the $M_2/M_1–L_2/L_1$ diagram correspond to the sample of the A. Poro et al. (2024b) study.

Figure 8(p) depicts the relationship between the orbital period and the system's absolute magnitude ($P–M_V$). The theoretical fit of this relationship is from the A. Poro et al. (2024b) study. Equation (10) was utilized to obtain absolute magnitude,

$$M_V = V_{\rm max} - 5\log(d) + 5 - A_V, \qquad (10)$$

where $V_{\rm max}$ is the maximum apparent magnitude of the system based on our observations, d is the star's distance resulting from Gaia DR3, and A_V is the result of the calculations in this study. The calculated M_V values are presented in Table 11. Apart from system J05, nine other systems are within the

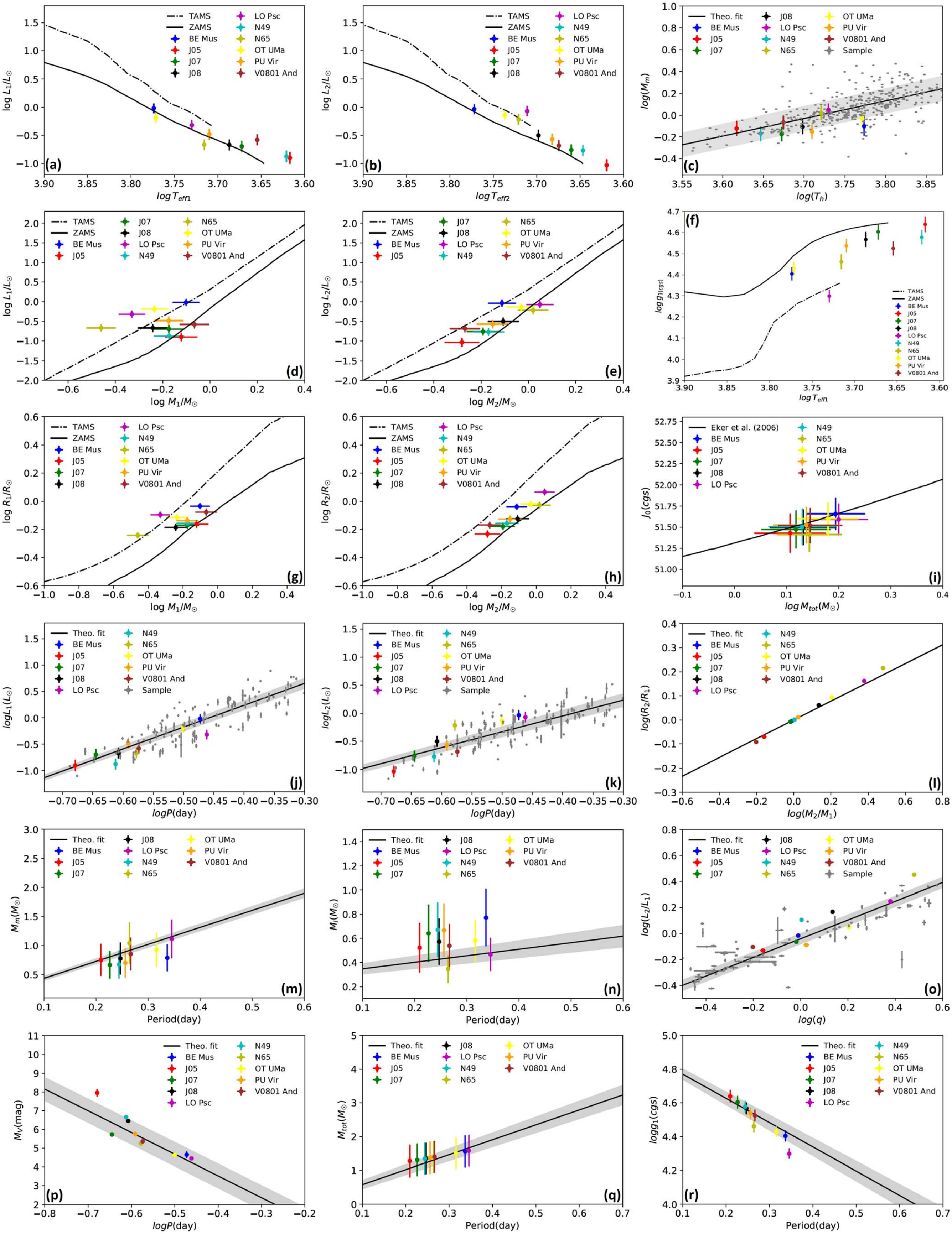

Figure 8. The position of the target systems in different diagrams of the parameter relationships.

uncertainty of the P–M_V fit. This shows that the high value of A_V can affect the calculations, especially if the Gaia DR3 parallax was used to estimate the absolute parameters.

Acknowledgments

This manuscript was prepared by the BSN project. Work by K.L. was supported by the National Natural Science Foundation of China (NSFC; No. 12273018) and by the Qilu Young Researcher Project of Shandong University. Ground-based observations of four systems were conducted with the cooperation of the Observatorio Astronómico Nacional on the Sierra San Pedro Mártir (OAN-SPM), Baja California, México. We used IRAF, which is distributed by the National Optical Astronomy Observatories and operated by the Association of Universities for Research in Astronomy, Inc., under a cooperative agreement with the National Science Foundation. We used data from the European Space Agency's mission Gaia.[20] This work includes data from the TESS mission observations. The NASA Explorer Program provides funding for the TESS mission. This paper used some results from the American Association of Variable Star Observers (AAVSO[21]). We appreciate the helpful comments from Shinjirou Kouzuma, Edwin Budding, and Ehsan Paki. Finally, we thank the referee for help in improving the paper.

Data Availability

Ground-based data are available in the paper's supplement.

ORCID iDs

Atila Poro https://orcid.org/0000-0002-0196-9732
Kai Li https://orcid.org/0000-0003-3590-335X
Raul Michel https://orcid.org/0000-0003-1263-808X
Angel Castro https://orcid.org/0000-0002-7832-5337
Eduardo Fernández Lajús https://orcid.org/0000-0002-9262-4456
Li-Heng Wang https://orcid.org/0009-0005-0485-418X
Jean-François Coliac https://orcid.org/0000-0003-0354-8568
Yasemin Aladağ https://orcid.org/0000-0002-6107-579X
Ailar Alizadehsabegh https://orcid.org/0000-0001-5768-0340
Fahri Alicavus https://orcid.org/0000-0002-1972-8400

References

Albayrak, B., Djurašević, G., Selam, S. O., Atanacković-Vukmanović, O., & Yılmaz, M. 2005, NewA, 10, 163
Astropy Collaboration, Price-Whelan, A. M., Lim, P. L., et al. 2022, ApJ, 935, 167
Astropy Collaboration, Price-Whelan, A. M., Sipőcz, B. M., et al. 2018, AJ, 156, 123
Astropy Collaboration, Robitaille, T. P., Tollerud, E. J., et al. 2013, A&A, 558, A33
Avvakumova, E. A., Malkov, O. Y., & Kniazev, A. Y. 2013, AN, 334, 860
Bellm, E. C., Kulkarni, S. R., Barlow, T., et al. 2019, PASP, 131, 068003
Binnendijk, L. 1970, VA, 12, 217
Butters, O. W., West, R. G., Anderson, D. R., et al. 2010, A&A, 520, L10
Castelli, F., & Kurucz, R. L. 2004, A&A, 419, 725
Chen, X., Wang, S., Deng, L., et al. 2020, ApJS, 249, 18
Collins, K. A., Kielkopf, J. F., Stassun, K. G., & Hessman, F. V. 2017, AJ, 153, 77
Conroy, K. E., Kochoska, A., Hey, D., et al. 2020, ApJS, 250, 34
Cox, A. N. 2000, Allen's Astrophysical Quantities (AN Cox ed)
Csizmadia, S., & Klagyivik, P. 2004, A&A, 426, 1001
Damerdji, Y., Klotz, A., & Boër, M. 2007, AJ, 133, 1470
Deb, S., & Singh, H. P. 2011, MNRAS, 412, 1787
Djurašević, G., Dimitrov, D., Arbutina, B., et al. 2006, PASA, 23, 154
Drake, A. J., Djorgovski, S. G., García-Álvarez, D., et al. 2014a, ApJ, 790, 157
Drake, A. J., Graham, M. J., Djorgovski, S. G., et al. 2014b, ApJS, 213, 9
Eggleton, P. P. 2012, JASS, 29, 145
Eker, Z., Bakış, V., Bilir, S., et al. 2018, MNRAS, 479, 5491
Eker, Z., Demircan, O., Bilir, S., & Karatas, Y. 2006, MNRAS, 373, 1483
Eker, Z., Demircan, O., & Bilir, S. 2008, MNRAS, 386, 1756
Essam, A., Saad, S. M., Nouh, M. I., et al. 2010, NewA, 15, 227
Flower, P. J. 1996, ApJ, 469, 355
Foreman-Mackey, D., Hogg, D. W., Lang, D., & Goodman, J. 2013, PASP, 125, 306
Gaia Collaboration, Montegriffo, P., Bellazzini, M., et al. 2023, A&A, 674, A33
Gazeas, K., Zola, S., Liakos, A., et al. 2021, MNRAS, 501, 2897
Gettel, S. J., Geske, M. T., & McKay, T. A. 2006, AJ, 131, 621
Girardi, L., Bressan, A., Bertelli, G., & Chiosi, C. 2000, A&AS, 141, 371
Green, G. M., Schlafly, E., Zucker, C., Speagle, J. S., & Finkbeiner, D. 2019, ApJ, 887, 93
Guinan, E. F., & Bradstreet, D. H. 1988, in NATO Advanced Study Institute (ASI) Series C, Formation and Evolution of Low Mass Stars, ed. A. K. Dupree & M. T. V. T. Lago, Vol. 241 (Berlin: Springer), 345
Guthnick, P., & Prager, R. 1933, AN, 249, 253
Hambálek, Ľ., & Pribulla, T. 2013, CoSka, 43, 27
Hiltner, W. A. 1962, Astronomical Techniques (Chicago, IL: Univ. Chicago Press)
Hoffman, D. I., Harrison, T. E., & McNamara, B. J. 2009, AJ, 138, 466
Huang, H.-P., Yu, Y.-X., Yu, T., Hu, K., & Xiang, F.-Y. 2021, RAA, 21, 120
Jayasinghe, T., Kochanek, C. S., Stanek, K. Z., et al. 2018, MNRAS, 477, 3145
Jenkins, J. M., Twicken, J. D., McCauliff, S., et al. 2016, Proc. SPIE, 9913, 99133E
Jiang, L., Qian, S.-B., Zhang, J., & Liu, N. 2015, PASJ, 67, 118
Kallrath, J., Milone, E. F., & Wilson, R. 2009, Eclipsing Binary Stars: Modeling and Analysis, Vol. 11 (Berlin: Springer)
Khruslov, A. V. 2007, PZP, 7, 6
Kouzuma, S. 2018, PASJ, 70, 90
Kouzuma, S. 2023, ApJ, 958, 84
Kreiner, J. M., Rucinski, S. M., Zola, S., et al. 2003, A&A, 412, 465
Kuiper, G. P. 1941, ApJ, 93, 133
Kwee, K. K. 1958, BAN, 14, 131
Kwee, K. K., & van Woerden, H. 1956, BAN, 12, 327
Latković, O., Čeki, A., & Lazarević, S. 2021, ApJS, 254, 10
Lee, J. W., Kim, C.-H., Han, W., Kim, H.-I., & Koch, R. H. 2004, MNRAS, 352, 1041
Li, K., Gao, X., Liu, X.-Y., et al. 2022, AJ, 164, 202
Li, K., Kim, C.-H., Xia, Q.-Q., et al. 2020, AJ, 159, 189
Li, K., Xia, Q.-Q., Kim, C.-H., et al. 2021, AJ, 162, 13
Li, K., Xia, Q.-Q., Michel, R., et al. 2019, MNRAS, 485, 4588
Li, L., & Zhang, F. 2006, MNRAS, 369, 2001
Li, L., Zhang, F., Han, Z., & Jiang, D. 2007, ApJ, 662, 596
Li, X.-Z., Zhu, Q.-F., Ding, X., et al. 2024, ApJS, 271, 32
Liu, X.-Y., Li, K., Michel, R., et al. 2023, MNRAS, 519, 5760
Lucy, L. B. 1967, ZAp, 65, 89
Lucy, L. B. 1968a, ApJ, 151, 1123
Lucy, L. B. 1968b, ApJ, 153, 877
Malkov, O. Y., Oblak, E., Snegireva, E. A., & Torra, J. 2006, A&A, 446, 785
Marsh, F. M., Prince, T. A., Mahabal, A. A., et al. 2017, MNRAS, 465, 4678
Masci, F. J., Laher, R. R., Rusholme, B., et al. 2019, PASP, 131, 018003
Mitnyan, T., Szalai, T., Bódi, A., et al. 2020, A&A, 635, A89
Nelson, R. H., & Robb, R. M. 2015, IBVS, 6134, 1
O'Connell, D. J. K. 1951, PRCO, 2, 85
Paki, E., & Poro, A. 2024, Ap, 67, 316
Pešta, M., & Pejcha, O. 2023, A&A, 672, A176
Poro, A., Baudart, S., Nourmohammad, M., et al. 2024d, RAA, 24, 055001
Poro, A., Blackford, M. G., Davoudi, F., et al. 2021, OAst, 30, 37
Poro, A., Hedayatjoo, M., Nastaran, M., et al. 2024a, NewA, 110, 102227
Poro, A., Paki, E., Alizadehsabegh, A., et al. 2024b, RAA, 24, 015002
Poro, A., Paki, E., Blackford, M. G., et al. 2022a, PASP, 134, 064201
Poro, A., Sarabi, S., Zamanpour, S., et al. 2022b, MNRAS, 510, 5315
Poro, A., Tanriver, M., Michel, R., & Paki, E. 2024c, PASP, 136, 024201
Poro, A., Tanriver, M., Sarvari, E., et al. 2024d, RAA, 24, 045018
Pribulla, T., Rucinski, S. M., Blake, R. M., et al. 2009, AJ, 137, 3655
Prša, A., Conroy, K. E., Horvat, M., et al. 2016, ApJS, 227, 29

[20] http://www.cosmos.esa.int/gaia
[21] https://www.aavso.org/

Qian, S. 2003, MNRAS, 342, 1260
Qian, S. B., Wang, J. J., Zhu, L. Y., et al. 2014, ApJS, 212, 4
Rahimi, J., Lashgari, E., Ghanbarzadehchaleshtori, M., et al. 2021, NewA, 84, 101499
Ricker, G. R., Latham, D. W., Vanderspek, R. K., et al. 2010, AAS Meeting Abstracts, 215, 450.06
Ricker, G. R., Winn, J. N., Vanderspek, R., et al. 2015, JATIS, 1, 014003
Rinner, C., Starkey, D., Demeautis, C., et al. 2003, IBVS, 5428, 1
Ruciński, S. M. 1969, AcA, 19, 245
Rucinski, S. M. 1992, AJ, 103, 960
Rucinski, S. M. 2000, AJ, 120, 319
Selam, S. O., Esmer, E. M., Şenavcı, H. V., et al. 2018, Ap&SS, 363, 34
Shappee, B. J., Prieto, J. L., Grupe, D., et al. 2014, ApJ, 788, 48
Soomandar, S., & Poro, A. 2024, NewA, 105, 102112
Sriram, K., Malu, S., Choi, C. S., & Vivekananda Rao, P. 2016, AJ, 151, 69
Stassun, K. G., Oelkers, R. J., Pepper, J., et al. 2018, AJ, 156, 102
Sun, W., Chen, X., Deng, L., & de Grijs, R. 2020, ApJS, 247, 50
Szalai, T., Kiss, L. L., Mészáros, S., Vinkó, J., & Csizmadia, S. 2007, A&A, 465, 943
Terrell, D., Gross, J., & Cooney, W. R. 2012, AJ, 143, 99
Terrell, D., & Wilson, R. E. 2005, Ap&SS, 296, 221
Tian, X.-M., Zhu, L.-Y., Qian, S.-B., Li, L.-J., & Jiang, L.-Q. 2018, RAA, 18, 020
Tody, D. 1986, Proc. SPIE, 627, 733
Tonry, J. L., Denneau, L., Flewelling, H., et al. 2018, ApJ, 867, 105
Torres, G. 2010, AJ, 140, 1158
Wadhwa, S. S., Landin, N. R., Kostić, P., et al. 2024, MNRAS, 527, 1
Weldrake, D. T. F., Sackett, P. D., Bridges, T. J., & Freeman, K. C. 2004, AJ, 128, 736
Williams, P. S., & Roxburgh, I. W. 1976, MNRAS, 176, 81
Yakut, K., & Eggleton, P. P. 2005, ApJ, 629, 1055
Yıldırım, M. F. 2022, RAA, 22, 055013
Yıldız, M. 2015, RAA, 15, 2244
Zhang, X.-D., & Qian, S.-B. 2020, MNRAS, 497, 3493
Zola, S., Gazeas, K., Kreiner, J. M., et al. 2010, MNRAS, 408, 464